J. Fluid Mech. (1994), *vol.* 269, *pp.* 323–351

The stability of a trailing-line vortex in compressible flow

By JILLIAN A. K. STOTT† AND PETER W. DUCK
Department of Mathematics, University of Manchester, Manchester, M13 9PL, UK

(Received 12 November 1992 and in revised form 12 January 1994)

We consider the inviscid stability of the Batchelor (1964) vortex in a compressible flow. The problem is tackled numerically and also asymptotically, in the limit of large (azimuthal and streamwise) wavenumbers, together with large Mach numbers. The nature of the solution passes through different regimes as the Mach number increases, relative to the wavenumbers. At very high wavenumbers and Mach numbers, the mode which is present in the incompressible case ceases to be unstable, whilst a new 'centre mode' forms, whose stability characteristics are determined primarily by conditions close to the vortex axis. We find that generally the flow becomes less unstable as the Mach number increases, and that the regime of instability appears generally confined to disturbances in a direction counter to the direction of the rotation of the swirl of the vortex.

Throughout the paper comparison is made between our numerical results and results obtained from the various asymptotic theories.

1. Introduction

In recent years there has been a good deal of interest in the stability of incompressible swirling vortex-type flows. Two important applications of this area of research are to the breakdown of trailing-line vortices behind aircraft and to tornadoes; this class of flow may also be applicable to flows inside turbines and compressors, to which the present work would be particularly relevant.

The earliest works in the area of the stability of swirling vortex flows include those of Lessen & Paillet (1974) and Lessen, Singh & Paillet (1974). In the former paper the stability of the Batchelor (1964) vortex was considered, at finite Reynolds numbers up to 150. In the second paper, the inviscid stability of this vortex was studied and revealed an increase in growth rate at increasingly large wavenumbers (with disturbances being most dangerous counter to the direction of the swirl).

Duck & Foster (1980) showed that for a given wavenumber a multiplicity of modes exists. Leibovich & Stewartson (1983) and Duck (1986) considered the limit of large wavenumber for this problem, and showed that a finite (maximum) growth rate was attained. The aforementioned studies suggested an upper and lower neutral value of axial wavenumber. The upper neutral point for large azimuthal wavenumber was treated by Stewartson & Capell (1985), who showed that the 'ring mode' structure of the unstable modes persisted near the upper neutral points. Stewartson & Brown (1985) considered these upper neutral points for order-one azimuthal wavenumbers, and found that in this case modes of centre-mode type could exist, similar to those

† Present address: School of Mathematics, University of New South Wales, Australia.

found in a related study on swirling Poiseuille flow (Stewartson & Brown 1984). The behaviour of the unstable modes, close to the lower neutral point, at large azimuthal wavenumber, was investigated by Stewartson & Leibovich (1987), who determined that in this case the instability disturbances were centred near the axis of the vortex.

More recently, viscous results have been presented at finite (but large) Reynolds numbers by Khorrami, Malik & Ash (1989) and Khorrami (1991). In this latter paper, it was shown that additional unstable modes exist, in which viscosity plays a destabilizing role. These modes were analysed using asymptotic methods by Duck & Khorrami (1991). The inviscid analysis is also applicable to other vortex profiles, including that of Long (1961), as studied by Foster & Duck (1982) and Foster & Smith (1989). Regions of instability for both the viscous and inviscid problem have been mapped out by Mayer & Powell (1992).

Little attention has been paid to the stability of compressible vortex flows of this type, even though we know from experiments that velocities are often higher in the core than in the free stream, so compressibility could strongly affect the character of the vortex, even at subsonic flight Mach numbers. On the other hand the area of compressible jet flow has been investigated for some years now, the work of Michalke (1971, 1984) being relevant here, although restricted to non-swirling flows. Compressible swirling jet flows have also received some attention; the work of Coleman (1989) should be mentioned, who studied the superposition of a Rankine vortex on a top-hat jet velocity field. More recently, Khorrami (1991) studied a compressible swirling axisymmetric jet, by assuming that the incompressible flow of Görtler (1954) and Loitsyanskii (1953) was applicable in the compressible regime.

In this paper, we take cylindrical polar coordinates, $(lx, l\hat{r}, \theta)$, with the x-axis lying along the axis of the vortex (which is taken to be axisymmetric), where l is some streamwise scale. We also take the flow far from the vortex centre to be directed along the x-direction. The velocity field is written as $U_s^* \boldsymbol{u} = U_s^*(u, v, w)$, the fluid density is $\rho_\infty^* \rho$, temperature $T_\infty^* T$, first and second coefficients of viscosity $\mu_\infty^* \mu$, $\mu_\infty^* \lambda$ respectively, and pressure $\rho_\infty^* U_s^{*2} p$. Here a superscript asterisk and a subscript ∞ denote dimensional and free-stream variables, respectively, and U_s^* is a velocity scale, defined below in (2.6), whilst U_∞^* is the free-stream velocity. We define the flow Reynolds number

$$Re = \frac{\rho_\infty^* U_s^* l}{\mu_\infty^*}, \tag{1.1}$$

and we have a flow Mach number given by

$$M = \frac{U_s^*}{(\gamma R^* T_\infty^*)^{\frac{1}{2}}}, \tag{1.2}$$

where γ is the ratio of specific heats and R^* the gas constant. We also define the Prandtl number to be

$$\sigma = \frac{\mu^* c_p}{\kappa^*}, \tag{1.3}$$

where κ^* is the thermal conductivity of the fluid.

The non-dimensional equations of continuity, momentum and energy may then be written

$$\frac{\partial \rho}{\partial t} + \nabla \cdot (\rho \boldsymbol{u}) = 0, \tag{1.4}$$

$$\rho\frac{\mathrm{D}\boldsymbol{u}}{\mathrm{D}t} = -\nabla p - \frac{1}{Re}\nabla\wedge[\mu(\nabla\wedge\boldsymbol{u})] + \frac{1}{Re}\nabla\cdot[(\lambda+2\mu)\nabla\cdot\boldsymbol{u}], \tag{1.5}$$

$$\rho\frac{\mathrm{D}h}{\mathrm{D}t} = \frac{\mathrm{D}p}{\mathrm{D}t} + \Phi + \frac{1}{\sigma Re}\nabla\cdot(\mu\nabla T), \tag{1.6}$$

where h is the enthalpy of the fluid, and Φ is the viscous dissipation. We also assume a perfect gas, in which case we have

$$p = \frac{\rho T}{\gamma M^2}. \tag{1.7}$$

In the following sections we consider first the basic flow (§2), and derive an asymptotic solution of the above equations of continuity, momentum and energy, valid for large Mach numbers. In §3 we consider the inviscid linear stability equations. In §4 we present a number of numerical results, guided by which, in §5 we develop asymptotic results for large axial and azimuthal wavenumbers; throughout this section we emphasize a comparison between our numerical and asymptotic results. In §6 a new class of mode, which is found to develop at sufficiently large Mach number, is considered. In §7 we present a number of conclusions arising from this work.

2. The basic flow

Let us consider the solution corresponding to Batchelors' (1964) similarity solution for a swirling wake flow, equivalent to a far downstream limit ($x \gg 1$) of the governing equations. We thus suppose that the solution comprises a uniform (free-stream) flow plus a relatively small steady perturbation, i.e.

$$u = \frac{U^*_\infty}{U^*_s} + \tilde{u}, \quad v = \tilde{v}, \quad w = \tilde{w}, \tag{2.1 a–c}$$

$$p = \frac{U^{*2}_\infty}{U^{*2}_s} + \tilde{p}, \quad T = 1+\tilde{T}, \quad \rho = 1+\tilde{\rho}. \tag{2.1 d–f}$$

The solution develops in much the same way as the incompressible case of Batchelor (1964) and it is found to leading order (i.e. neglecting tilde-squared terms) that

$$\tilde{u} = \frac{1}{U^*_s}\left(-\frac{C_0^2 U^*_\infty \log(x\,Re_\infty)}{8x\nu^{*2}_\infty Re_\infty} Q_1(\eta) + \frac{C_0^2 U^*_\infty}{8x\nu^{*2}_\infty Re_\infty} Q_2(\eta) - \frac{LU^{*2}_\infty \mathrm{e}^{-\eta}}{8x\nu^{*2}_\infty Re_\infty}\right), \tag{2.2}$$

$$\tilde{v} = 0, \tag{2.3}$$

$$\tilde{w} = \frac{C_0 Re_\infty^{\frac{1}{2}}}{2(x\eta)^{\frac{1}{2}}U^*_s}(1-\mathrm{e}^{-\eta}), \tag{2.4}$$

where

$$\eta = \hat{r}^2 Re_\infty/4x, \tag{2.5}$$

$$U^*_s = \frac{C_0^2 U^*_\infty}{8x\nu^{*2}_\infty Re_\infty}\log(xRe_\infty) + \frac{LU^{*2}_\infty}{8x\nu^{*2}_\infty Re_\infty}, \tag{2.6}$$

and

$$Q_1(\eta) = \mathrm{e}^{-\eta}, \quad Q_2(\eta) = \mathrm{e}^{-\eta}[\log\eta + \mathrm{ei}(\eta) - 0.867] + 2\mathrm{ei}(\eta). \tag{2.7 a, b}$$

C_0 and L are constants and Re_∞ is the free-stream Reynolds number defined by

$$Re_\infty = \rho^*_\infty U^*_\infty l/\mu^*_\infty. \tag{2.8}$$

To the order that we are working it is admissible to take the viscosities and Prandtl number as constants, although any higher-order theories would require taking variations of these quantities into account. We find that

$$\tilde{p} = \frac{C_0^2 U_\infty^{*2}}{8x\nu_\infty^{*2} U_s^{*2} Re_\infty}\left[\frac{(1-e^{-\eta})^2}{\eta} + 2\mathrm{ei}(\eta) - 2\mathrm{ei}(2\eta)\right], \tag{2.9}$$

whilst the temperature perturbation is governed by the following equation:

$$\frac{1}{\sigma}\frac{d^2\tilde{T}}{d\xi^2} + \left(\frac{1}{\sigma\xi} + \frac{\xi}{2}\right)\frac{d\tilde{T}}{d\xi} + \tilde{T} = -(\gamma-1)\frac{M_\infty^2}{8\nu_\infty^{*2} x\, Re_\infty}\left[\frac{10C_0^2}{\xi^4}(1-e^{-\xi^2/4})^2 + \tfrac{1}{2}C_0^2 e^{-\xi^2/2}\right]. \tag{2.10}$$

The general solution of this is given by

$$\begin{aligned}\tilde{T} = e^{-\sigma\xi^2/4}\Bigg(&\tfrac{1}{2}A\,\mathrm{ei}(\tfrac{1}{4}\sigma\xi^2) + B + \frac{(\gamma-1)M_\infty^2 C_0^2}{8x\nu_\infty^{*2} Re_\infty}\Bigg[\mathrm{ei}((\tfrac{1}{4}\sigma-\tfrac{1}{4})\xi^2)\\ &+\int_\infty^\xi\Bigg(-8\sigma\frac{e^{\sigma\xi^2/4}}{\xi^2} + 16\sigma\frac{e^{(\sigma-1)\xi^2/4}}{\xi^2}\\ &+\frac{8\sigma\pi^{\frac{1}{2}}}{\xi}e^{\sigma\xi^2/4}\,\mathrm{erf}(\tfrac{1}{2}\xi) - 8\frac{e^{(\sigma/4-\frac{1}{2})\xi^2}}{\xi^2} - 4\frac{\sigma 2\pi^{\frac{1}{2}}}{x}e^{\sigma\xi^2/4}\,\mathrm{erf}(\xi/2^{\frac{1}{2}})\Bigg)d\xi\\ &+\int_\infty^\xi e^{\sigma\xi^2/4}\int_\infty^\xi\frac{1}{\xi_1}\Bigg(-2\sigma\Bigg(-2e^{\xi_1^2/4} + 2 - \xi_1^2 e^{\xi_1^2/4}\,\mathrm{ei}(\tfrac{1}{4}\xi_1^2)\\ &+\xi_1^2 e^{\xi_1^2/4}\,\mathrm{ei}(\tfrac{1}{2}\xi_1^2)\Bigg) + \frac{e^{-\xi_1^2/4}}{\xi_1}\Bigg)d\xi_1\,d\xi\Bigg]\Bigg),\end{aligned} \tag{2.11}$$

where A and B are constants (which we tacitly take to be order-one quantities), which depend on the history of the flow, $\xi = 2\eta^{\frac{1}{2}}$, $\mathrm{ei}(z)$ and $\mathrm{erf}(z)$ are the exponential integral and the error function, respectively, defined in the normal manner, and M_∞ is the free-stream Mach number defined by

$$M_\infty = \frac{U_\infty^*}{(\gamma R^* T_\infty^*)^{\frac{1}{2}}} = \frac{U_\infty^*}{U_s^*}M. \tag{2.12}$$

Note that we expect $M_\infty \gg M$. We also find it useful for the remainder of the paper to define the lengthscale

$$r = \eta^{\frac{1}{2}} = \hat{r}/r_s, \tag{2.13}$$

where $r_s = (4x/Re_\infty)^{\frac{1}{2}}$ is the characteristic radial lengthscale.

In the following section we consider the inviscid stability equations.

3. The stability equations

We take the general basic state to be $u = U(r)$, $v = 0$, $w = W(r)$, $T = T_0(r)$, $p = p_0(r)$, $\rho = \rho_0(r)$ and consider small-amplitude perturbations to this flow; we write

$$u = U(r) + \delta F(r)E + O(\delta^2), \quad v = \mathrm{i}\delta G(r)E + O(\delta^2), \quad w = W(r) + \delta H(r)E + O(\delta^2), \tag{3.1a–c}$$

$$p = p_0(r) + \delta P(r)E + O(\delta^2), \quad T = T_0(r) + \delta\tau(r)E + O(\delta^2), \quad \rho = \rho_0(r) + \delta\Gamma(r)E + O(\delta^2), \tag{3.1d–f}$$

where $\delta \ll 1$ and

$$E = \exp[\mathrm{i}(\alpha x/r_s + n\theta - \alpha ct/r_s)]. \tag{3.1g}$$

The governing stability equations, neglecting the effects of viscosity are then

$$\Gamma\phi+\rho_0\left(\alpha F+G'+\frac{G}{r}+\frac{nH}{r}\right)+G\rho_0'=0, \tag{3.2}$$

$$\rho_0\phi F+\rho_0 U'G=-\alpha P, \tag{3.3}$$

$$\rho_0\phi G+\rho_0\frac{2WH}{r}+\frac{\Gamma W^2}{r}=P', \tag{3.4}$$

$$\rho_0\phi H+\rho_0\left(W'+\frac{W}{r}\right)G=-\frac{nP}{r}, \tag{3.5}$$

$$\rho_0\phi\tau+\rho_0 GT_0'(r)-(\gamma-1)M^2(\phi P+Gp_0')=0, \tag{3.6}$$

$$\gamma M^2P=\Gamma T_0+\tau\rho_0, \tag{3.7}$$

where we have written

$$\phi=\alpha(U-c)+nW/r, \tag{3.8}$$

and primes denote differentiation with respect to r. Note that (3.1), and (3.2)–(3.7) all implicitly assume that the axial scale for the perturbation quantities is considerably shorter than any developmental lengthscale for the basic flow, as is the case if $r_s \ll 1$.

Equations (3.2)–(3.7) may be combined to yield the following two first-order equations:

$$\frac{\mathrm{d}G}{\mathrm{d}r}=\left[\frac{n(rW)'+\alpha r^2U'}{r^2\phi}-\frac{p_0'}{\gamma p_0}-\frac{1}{r}\right]G+\frac{1}{\rho_0}\left[\frac{(\alpha^2r^2+n^2)}{r^2\phi}-\frac{\phi M^2}{T_0}\right]P, \tag{3.9}$$

$$\frac{\mathrm{d}P}{\mathrm{d}r}=\rho_0\left[\phi-\frac{(W^2r^2)'}{r^3\phi}-\frac{W^2}{r\phi}\left(\frac{\rho_0'}{\rho_0}-\frac{p_0'}{\gamma p_0}\right)\right]G-\left[\frac{2nW}{r^2\phi}-\frac{W^2M^2}{rT_0}\right]P. \tag{3.10}$$

These equations are somewhat similar to those considered by Michalke (1971), in the context of jet flows, if the swirl velocity is neglected.

Let us now consider the specific basic flow of the trailing-line vortex, as discussed in the previous section. Equations (2.1) and (2.3)–(2.5) may be substituted into (3.9), (3.10). If we then assume $|\delta| \ll |(1/x)\log x|$, use the fact that a simple transformation and inversion of the axial velocity only affects the frequency of the stability analysis, and does not change the amplification factor c_i (where $c=c_r+\mathrm{i}c_i$) and note that $\tilde{p}$, $\tilde{\rho}$ and $\tilde{T}$ are an order of $O(\log x)$ smaller than $\tilde{u}$ and $\tilde{w}$, then in terms of the similarity variable defined by (2.12), the basic flow may be taken to be

$$U=\mathrm{e}^{-r^2}, \quad W=\frac{q}{r}(1-\mathrm{e}^{-r^2}), \quad V=0, \tag{3.11a–c}$$

$$\rho_0=1, \quad p_0=1/\gamma M^2, \quad T_0=1, \tag{3.12a–c}$$

where q is an order-one (swirl) parameter, and we have effectively scaled velocities with respect to U_s^*.

Equations (3.9) and (3.10) reduce to

$$\frac{\mathrm{d}G}{\mathrm{d}r}=\left[\frac{n(rW)'+\alpha r^2U'}{r^2\phi}-\frac{1}{r}\right]G+\left[\frac{\alpha^2r^2+n^2}{r^2\phi}-\phi M^2\right]P, \tag{3.13}$$

$$\frac{\mathrm{d}P}{\mathrm{d}r}=\left[\phi-\frac{(W^2r^2)'}{r^3\phi}\right]G-\left[\frac{2nW}{r^2\phi}-\frac{W^2M^2}{r}\right]P. \tag{3.14}$$

The boundary conditions to be applied are then

$$\left.\begin{aligned} P(0) = 0, \quad n \neq 0; \quad P'(0) = 0, \quad n = 0, \\ G(0) = 0, \quad |n| \neq 1; \quad G'(0) = 0, \quad |n| = 1, \\ \text{and} \qquad G(r), P(r) \text{ bounded as } r \to \infty. \end{aligned}\right\} \tag{3.15}$$

Equations (3.13) and (3.14) may be combined to eliminate G, yielding the following second-order equation for P:

$$\begin{aligned} &P_{rr} + P_r\left\{\frac{2nW}{r^2\phi} - \frac{W^2M^2}{r} + \frac{1}{r} - \left[\phi - \frac{(W^2r^2)'}{r^3\phi}\right]'\Big/\left[\phi - \frac{(W^2r^2)'}{r^3\phi}\right] - \frac{[\alpha r^2U' + n(rW)']}{r^2\phi}\right\} \\ &+ P\left\{\left[\frac{2nW}{r^2\phi} - \frac{W^2M^2}{r}\right]' - \left[\frac{2nW}{r^2\phi} - \frac{W^2M^2}{r}\right]\left[\phi - \frac{(W^2r^2)'}{r^3\phi}\right]'\Big/\left[\phi - \frac{(W^2r^2)'}{r^3\phi}\right]\right. \\ &\left. + \left(\frac{1}{r} - \frac{[\alpha r^2U' + n(rW)']}{r^2\phi}\right)\left[\frac{2nW}{r^2\phi} - \frac{W^2M^2}{r}\right] - \left[\frac{\alpha^2r^2 + n^2}{r^2\phi} - \phi M^2\right]\left[\phi - \frac{(W^2r^2)'}{r^3\phi}\right]\right\} = 0. \end{aligned} \tag{3.16}$$

Setting $M = 0$ clearly reduces (3.13), (3.14) and (3.16) to the incompressible problem, as considered by Lessen *et al.* (1974), Duck & Foster (1980), Leibovich & Stewartson (1983) and Duck (1986). It is also possible to be rather more precise regarding the behaviour of the solution as $r \to \infty$; this takes the form

$$\frac{dG}{dr} \pm \alpha(1 - c^2M^2)^{\frac{1}{2}}G = 0, \tag{3.17}$$

$$\frac{dP}{dr} \pm \alpha(1 - c^2M^2)^{\frac{1}{2}}P = 0, \tag{3.18}$$

where positive signs are taken for $\mathrm{Re}\{(1 - c^2M^2)^{\frac{1}{2}}\} > 0$, and vice versa, to ensure boundedness as $r \to \infty$.

The 'order-one' problem requires a fully numerical solution, which we consider in the following section, prior to considering various asymptotic limits of this system of equations, which permit some analytical progress.

4. Numerical results

The system was treated numerically using four different techniques. The first was based on the method of Duck & Foster (1980), in which the system (3.16) was approximated by second-order central differences, with conditions (3.17) and (3.18) imposed at a finite radial value $r = r_{max}$, taken sufficiently large not to substantially affect the result. The determinant of the system was then forced to zero by adjusting the complex wave speed c (using Newton iteration).

The second method was based on a fourth-order Runge–Kutta scheme; conditions (3.17) and (3.18) were approximated by imposing boundary conditions at a finite radial value $r = r_{max}$, where this value was again taken sufficiently large to not substantially affect the numerical results. The computations were performed by shooting the solution towards $r = 0$ and were not necessarily confined to the real r-axis. The value of c was adjusted (again using Newton iteration), to ensure the correct behaviour of the solution as $r \to 0$.

The third method used was based on the first, but was a global finite difference

method. Using this finite-difference scheme, then by defining two additional quantities $\hat{G} = cG, \hat{P} = cP$ at each grid point, it is possible to write the resulting scheme in the form

$$(\boldsymbol{A} - c\boldsymbol{B})\, x = 0, \tag{4.1}$$

where

$$x = [\{G\}, \{P\}, \{\hat{G}\}, \{\hat{P}\}]^T, \tag{4.2}$$

and $[\,]^T$ denotes the transpose of a vector. This scheme has the obvious advantage of generating $4N$ eigenvalues (where N is the number of grid points), simultaneously. The principle disadvantages are: (i) it is not possible to use (3.17) or (3.18) because of the nonlinearity of c, and consequently Dirichlet boundary conditions were applied instead at the outer edge of the computational domain; and (ii) the scheme requires rapidly increasing computational resources (both in storage and time) as N increases.

The fourth scheme implemented was a Chebyshev spectral collocation scheme, based on that of Khorrami *et al.* (1989). This was a global method, which generally gave very accurate eigenvalues, but also yielded a large number of spurious eigenvalues, a feature found in many spectral schemes.

The first (finite-difference) scheme was quick and robust, but because of its 'local' nature, mode jumping was often experienced due to the frequent close proximity of neighbouring modes, as discussed later in the paper. The second (Runge–Kutta) scheme was also quite fast, and had the advantage of being able to compute neutral and near-neutral modes (and even stable modes) by contour indentation, but again because it involved local searching was prone to mode jumping. The third scheme, namely the global finite-difference scheme, which proved to be very robust, produced few, if any spurious (i.e. non-physical) modes, and generated many eigenvalues simultaneously because of its global nature. Consequently our results were generally computed using the first scheme with the third scheme used to obtain approximate values for the eigenvalues, and to check on mode existence and ordering.

We now present a few numerical results to give some indication of the effects of variation of certain of the important parameters. Here, and indeed in all our calculations we chose $\gamma = 1.4$, $q = 0.8$. Further, we generally found that $r_{max} = 10$ was more than sufficient for graphical accuracy, with $\Delta r = 0.00625$.

Figure 1 (*a–c*) shows the variation of growth rate (αc_i) with α for the case $M = 3$, with $n = -1, -2, -3$ respectively. These results (and all those presented in this paper) are accurate to within the graphical accuracy of the figures. Because of the great multiplicity of these modes, we show just the first few (i.e. most unstable) modes. From the outset it should be stated that all our results relate to negative values of n; in general, we believe that instabilities are almost exclusively confined to this region of parameter space, with perhaps a few minor exceptions. (Lessen *et al.* 1974 have presented a few incompressible results for $n = +1$, for very small swirl parameters.) We certainly expect the largest growth rates to be confined to the negative values of n.

We see in figure 1 (and in other computed results, not presented here) the following general trends: (i) an increase in growth rates as $-n$ increases; (ii) an apparent cut-off value of α above which no unstable modes exist; (iii) a tendency for the maximum growth rate to be attained at an increasing value of α as $-n$ is increased; (iv) many modes of instability. We also note that there are instances where the growth rate which is not the least stable mode, locally exceeds that of a globally more unstable mode (particularly as α approaches the neutral points). This implies a number of mode crossings; this type of behaviour is rarely seen in incompressible studies, and serves to further complicate the computation of such modes.

In figure 2 (*a–e*) growth rates for the case $M = 5$ with $n = -1, -2, -3, -4, -5$

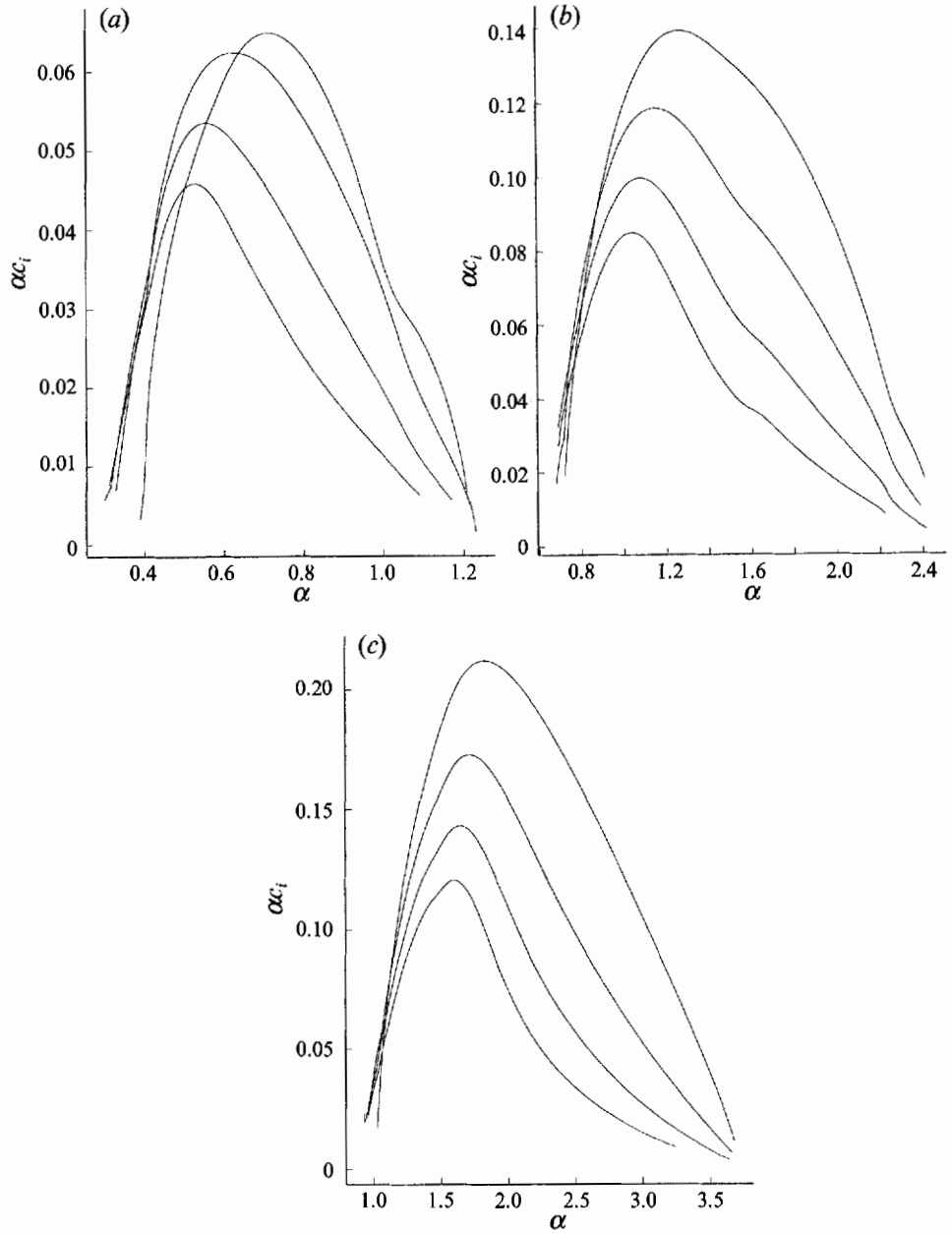

FIGURE 1. Variation of growth rate with α for $M = 3$: (*a*) $n = -1$, (*b*) $n = -2$, (*c*) $n = -3$.

respectively are presented. The trends (i)–(iv) described above are again observed, together with the result that for corresponding n and α the growth rates of $M = 5$ are substantially reduced compared to $M = 3$. Further the upper limit of α of the instability appears to be quite independent of M, and §6 confirms this observation.

These results suggest a number of interesting features, and in the following sections we mount a systematic study for increasing M, when $(-n) \gg 1$.

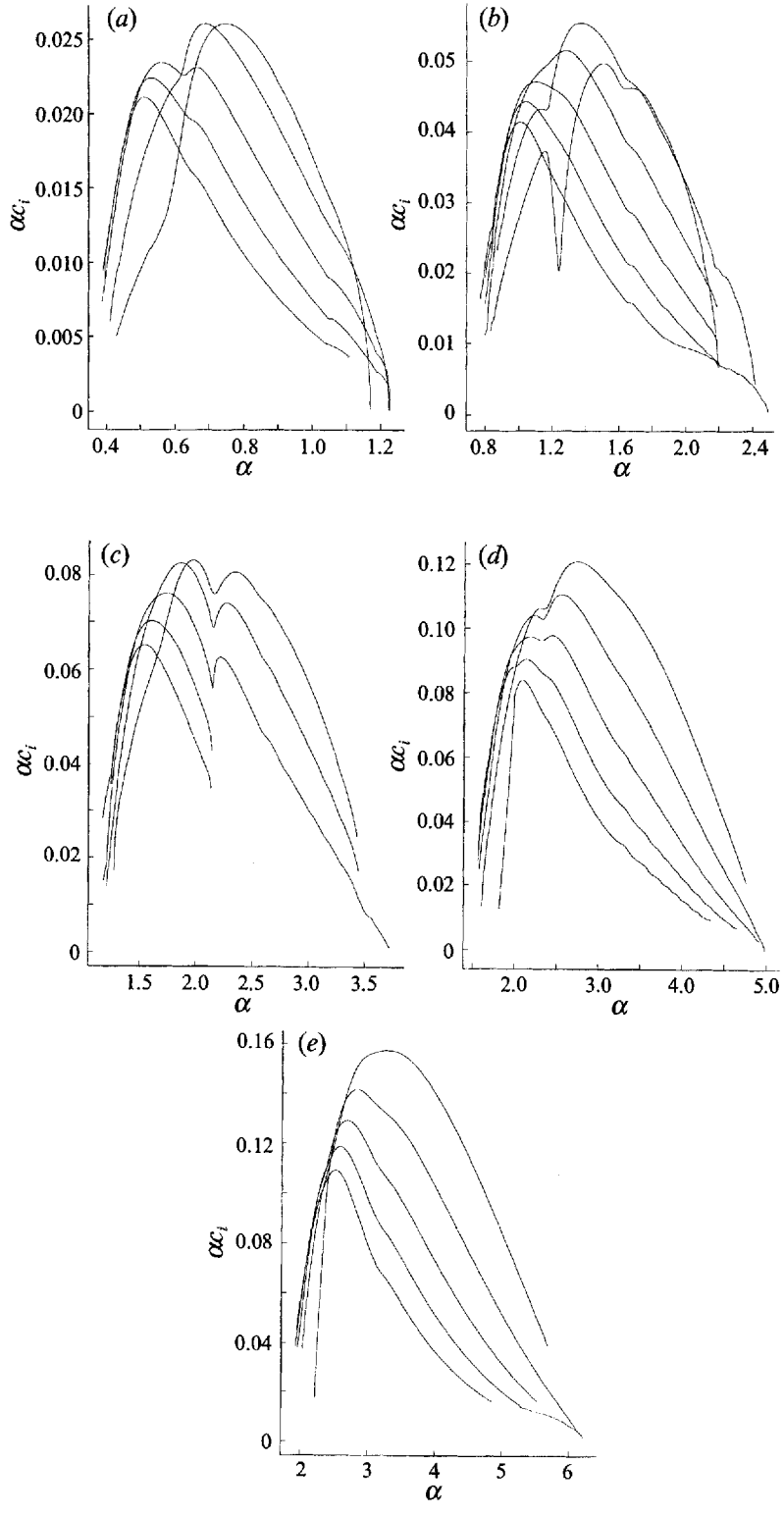

FIGURE 2. Variation of growth rate with α for $M = 5$: (*a*) $n = -1$, (*b*) $n = -2$, (*c*) $n = -3$, (*d*) $n = -4$, (*e*) $n = -5$.

5. Asymptotic results, $-n \gg 1$

5.1. $M = O(1)$

It turns out that for this order of Mach number, to the orders to which we concern ourselves, the solution (in particular for the complex wave speed) remains unchanged from the $-n \gg 1$ solution of the incompressible case, as considered by Leibovich & Stewartson (1983) and Duck (1986). However, since this solution forms a basis for the following subsections, we outline, briefly, the form of the structure in this case; full details can be found in the aforementioned papers. We have that

$$\alpha = n\bar{\alpha}, \quad \bar{\alpha} = O(1), \tag{5.1}$$

and the complex wave speed develops as

$$c = c_0 + \frac{c_1}{n} + \frac{c_2}{|n|^{\frac{3}{2}}} + \ldots. \tag{5.2}$$

Then generally

$$\phi = n\phi_0 + \phi_1 \frac{\phi_2}{|n|^{\frac{1}{2}}} + \ldots, \tag{5.3}$$

where

$$\phi_0 = \bar{\alpha}(U(r) - c_0) + W(r)/r. \tag{5.4}$$

However, the solution is found to be concentrated about points $r = r_0$ (critical points) where

$$\phi_0(r = r_0) = 0. \tag{5.5}$$

It turns out that r_0 must in fact also be a turning point, and so

$$\phi_0'(r_0) = 0, \tag{5.6}$$

i.e.

$$\bar{\alpha}U'(r_0) + (W/r)_0' = 0 \tag{5.7}$$

(where a subscript zero here and hereafter denotes evaluation at $r = r_0$). Equation (5.7) then serves to determine r_0, and hence c_0 may be determined from (5.5). The key lengthscale in the neighbourhood of the critical layer is given by

$$R = (r - r_0)|n|^{\frac{3}{4}}, \tag{5.8}$$

and then on this scale

$$\phi = \phi_1 - \frac{\operatorname{sign}(n)}{|n|^{\frac{1}{2}}}\{-\bar{\alpha}c_2 + \tfrac{1}{2}\phi_0''(r_0)\, R^2\} + O(n^{-1}), \tag{5.9}$$

where

$$\phi_1 = -\bar{\alpha}c_1, \tag{5.10}$$

$$\phi_0''(r_0) = \frac{\mathrm{d}^2}{\mathrm{d}r^2}[\phi_0(r)]_{r=r_0}. \tag{5.11}$$

For consistency it was shown by Leibovich & Stewartson (1983) and Duck (1986) that

$$c_1^2 = \frac{(W^2 r^2)_0'}{r_0^3 \bar{\alpha}^2} - \frac{[(rW)_0' + \bar{\alpha} r_0^2 U_0']^2}{(1 + \bar{\alpha}^2 r_0^2) r_0^2 \bar{\alpha}^2}. \tag{5.12}$$

Further, on the $R = O(1)$ scale the eigenfunctions scale as

$$P = \bar{P} + \ldots, \quad G = n\bar{G} + \ldots, \tag{5.13a, b}$$

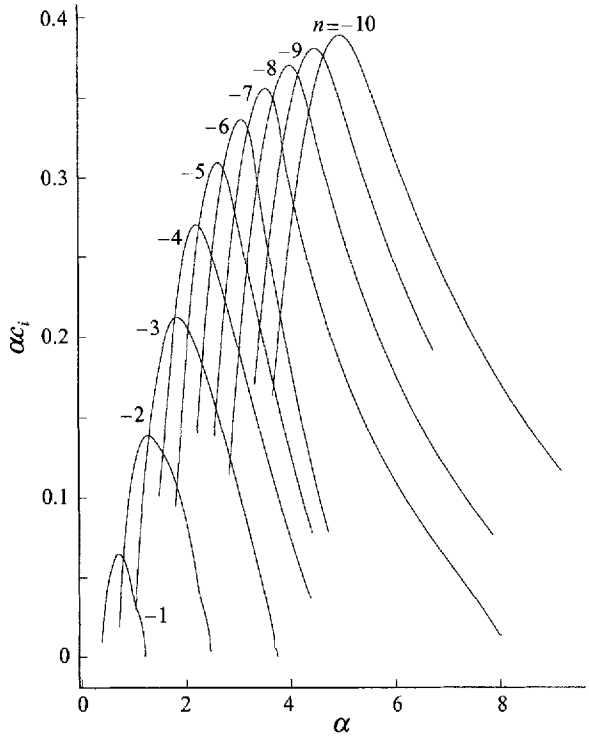

FIGURE 3. Variation of growth rate with α: computed most dangerous modes for $M = 3$, $n = -1$ to -10.

and then $\bar{P}(R)$ is described by

$$\bar{P}_{RR} - \left\{ 2\left[\frac{c_2}{c_1} - \frac{\phi_0''(r_0)\, R^2}{2\bar{\alpha} c_1} \right] \frac{\text{sign}\,(n)(1+\bar{\alpha}^2 r^{2GL0})}{r_0^2} \right\} \bar{P} = 0, \tag{5.14}$$

or

$$\bar{P}_{\xi\xi} - \left\{ \tfrac{1}{4}\xi^2 + \frac{\lambda_0 c_2}{2(\lambda_1)^{\frac{1}{2}}} \right\} \bar{P} = 0, \tag{5.15}$$

where we have written $\xi = \sqrt{2}\lambda_1^{\frac{1}{4}} R$, with

$$\lambda_0 = \frac{2}{c_1} \text{sign}\,(n) \frac{(1+\bar{\alpha}^2 r_0^2)}{r_0^2} \quad \text{and} \quad \lambda_1 = \frac{-\lambda_0 \phi_0''(r_0)}{2\bar{\alpha}}. \tag{5.16}$$

Equation (5.15) has a solution which may be written in terms of Weber parabolic cylinder functions, $D_m(\xi)$, and so if we demand that the solution decays as $|\xi| \to \infty$, then m must be an integer, yielding the following result for c_2:

$$c_2 = -\frac{(\lambda_1)^{\frac{1}{2}}}{\lambda_0}(1+2m), \quad m = 0, 1, 2, \ldots. \tag{5.17}$$

Figure 3 shows the variation of growth rates for $M = 3$, for $n = -1$ (the least-unstable mode shown) up to $n = -10$ (the most unstable mode shown) as computed for the full system; in all cases the most unstable mode for each value of n is shown. Using the asymptotic results above, we show the corresponding results in figure 4 (in particular

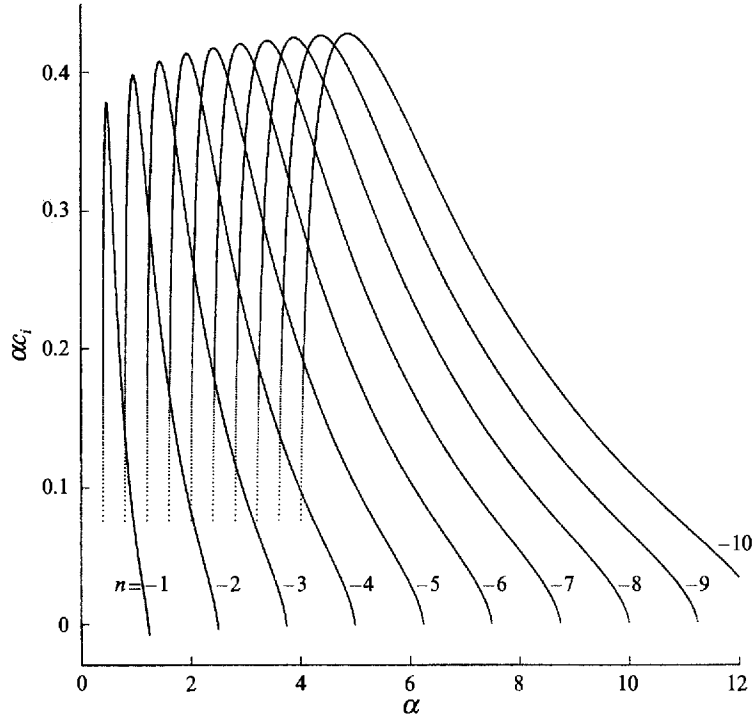

FIGURE 4. Variation of growth rate with α: asymptotic most dangerous modes using §5.1 results for $M = 3$, $n = -1$ to -10.

we set $m = 0$ in (5.17)). The comparison between figures 3 and 4 reveals good agreement in the growth rates at larger values of $-n$, although at smaller values of $-n$, comparison is less good than the comparison of incompressible numerical and asymptotic results. This less satisfactory agreement may be attributed directly to the effects of compressibility, but for $|n|$ sufficiently large, the asymptotic results presented in this subsection are ultimately approached.

In the following subsection we begin to incorporate compressibility into our asymptotic description.

5.2. $M = O(|n|^{\frac{1}{4}})$

The key equation (5.14) was obtained by taking the $O(|n|^{\frac{3}{4}})$ terms in (3.16). If $|n| \gg 1$, and we now permit M to grow in magnitude, additional terms will ultimately enter (5.14) when

$$M = |n|^{\frac{1}{4}}\tilde{M}, \quad \tilde{M} = O(1), \tag{5.18}$$

when the coefficient of $\bar{P}$ will include the effects of compressibility. The modified equation is then

$$\bar{P}_{RR} - \operatorname{sign}(n)\left\{2\left[\frac{c_2}{c_1} - \frac{\phi_0''(r_0)R^2}{2\bar{\alpha}c_1}\right]\frac{(1+\bar{\alpha}^2 r_0^2)}{r_0^2} + \left[\frac{(rW)_0' + \bar{\alpha}r_0^2 U_0'}{\bar{\alpha}c_1 r_0^2}\right]\left(\frac{W_0^2\tilde{M}^2}{r_0}\right)\right\}\bar{P} = 0. \tag{5.19}$$

All other quantities (specifically c_0 and c_1) remain unchanged from those evaluated previously. This equation may be transformed to the same form as (5.15), namely

$$\bar{P}_{\xi\xi} - \left\{\tfrac{1}{4}\xi^2 + \left(\frac{\lambda_0 c_2 + \lambda_2}{2(\lambda_1)^{\frac{1}{2}}}\right)\right\}\bar{P} = 0, \tag{5.20}$$

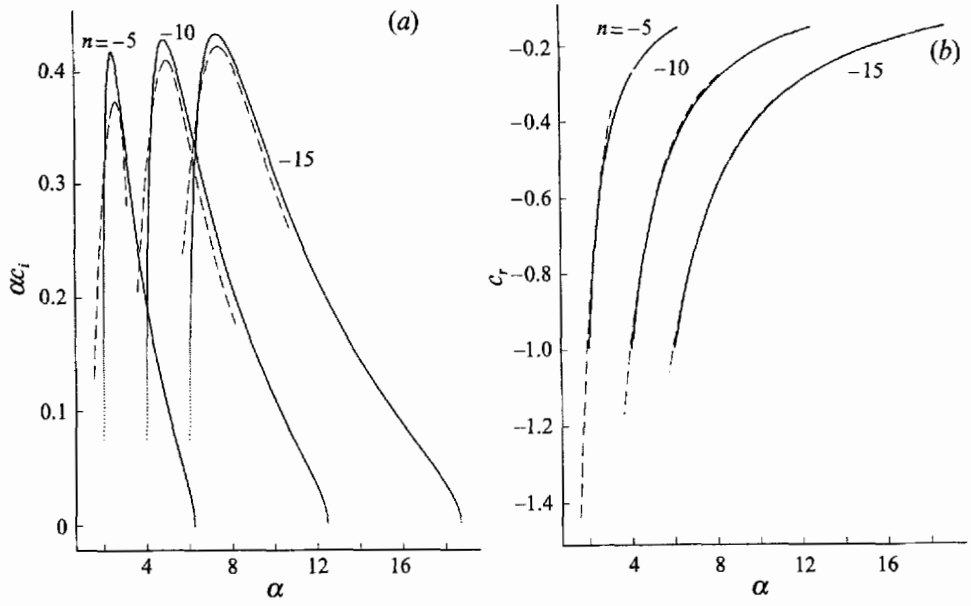

FIGURE 5. Variation of (*a*) growth rate c_i, and (*b*) c_r, with α, for $n = -5, -10, -15$, $M = |n|^{\frac{1}{3}}$: – – –, numerical results; ——, asymptotic results.

where λ_0 and λ_1 are given by (5.16), whilst

$$\lambda_2 = \text{sign}\,(n)\left[\frac{(rW)_0' + \bar{\alpha} r_0^2 U_0'}{\bar{\alpha} r_0^2 c_1}\right]\left(\frac{W_0^2 \tilde{M}^2}{r_0}\right). \tag{5.21}$$

Consequently, using our previous arguments

$$c_2 = -\left\{\frac{(\lambda_1)^{\frac{1}{3}}(1+2m)+\lambda_2}{\lambda_0}\right\}, \quad m = 0, 1, 2, \ldots. \tag{5.22}$$

Figure 5(*a*) shows a comparison of 'exact' growth rates (obtained using the numerical approach of §4), shown as a broken line, with the asymptotic results of this subsection; here, the chosen values of n are -5, -10 and -15 and we set $M = |n|^{\frac{1}{4}}$, i.e. $\tilde{M} = 1$ in each case. The agreement is satisfactory, and improves as n increases. Figure 5(*b*) shows the corresponding comparison for c_r; in this case the agreement is excellent.

5.3. $M = O(|n|^{\frac{3}{5}})$

As M (and hence $\tilde{M}$) increase in magnitude, the 'λ_2 component' of c_2 increases (as $\tilde{M}^2$) and becomes sufficiently larger than the 'λ_1 component'. Simultaneously, the coefficient of P_r in (3.16) will grow, and further terms in the coefficient of P will become significant. The next important regime for M is when

$$M = |n|^{\frac{3}{5}}\tilde{\tilde{M}}, \quad \tilde{\tilde{M}} = O(1). \tag{5.23}$$

Although the key radial scale remains $R = O(1)$ (see (5.8)), the series development of c and $\phi(R)$ is now altered, and is instead

$$c = c_0 + \frac{c_1}{n} + \frac{c_2}{|n|^{\frac{5}{4}}} + \frac{c_3}{|n|^{\frac{3}{2}}} + \ldots, \tag{5.24}$$

and therefore

$$\phi = \phi_1 + \frac{\phi_2}{|n|^{\frac{1}{4}}} + \frac{\phi_3}{|n|^{\frac{1}{2}}} + \ldots$$

$$= -\bar{\alpha}c_1 - \frac{1}{|n|^{\frac{1}{4}}}\bar{\alpha}c_2 \operatorname{sign}(n) + \frac{1}{|n|^{\frac{1}{2}}}\{-\bar{\alpha}c_3 \operatorname{sign}(n) + \tfrac{1}{2}\phi_0''(r_0)\, R^2\} + \ldots. \tag{5.25}$$

Considering $O(|n|^{\frac{3}{4}})$ quantities in (3.16) requires that the sum of these terms is zero, and so this leads to

$$c_2 = -\operatorname{sign}(n)\frac{\tilde{\tilde{M}}^2 W_0^2}{2\bar{\alpha}r_0}\left[\frac{(rW)_0' + \bar{\alpha}r_0^2 U_0'}{1+\bar{\alpha}^2 r_0^2}\right]. \tag{5.26}$$

The equation for $\bar{P}(R)$ is again obtained by taking the $O(|n|^{\frac{3}{2}})$ terms in (3.16), namely

$$\bar{P}_{RR} - \frac{\tilde{\tilde{M}}^2 W_0^2}{r_0}\bar{P}_R - \left\{\frac{1+\bar{\alpha}^2 r_0^2}{r_0^2}\left[2\frac{\phi_3}{\phi_1} + \frac{2\phi_2^2}{\phi_1^2}\right]\right.$$

$$\left. + \operatorname{sign}(n)\frac{\tilde{\tilde{M}}^2 W_0^2}{r_0}\left[\frac{(rW)_0' + \bar{\alpha}r_0^2 U_0'}{r_0^2 \phi_1}\right]\frac{\phi_2}{\phi_1}\right\}\bar{P} = 0. \tag{5.27}$$

Using the standard transformation

$$\bar{P}(R) = \bar{P}^*(R)\exp\left[\frac{1}{2}\frac{\tilde{\tilde{M}}^2 W_0^2 R}{r_0}\right], \tag{5.28}$$

then

$$\bar{P}^*_{RR} - \left\{2\operatorname{sign}(n)\left(\frac{c_3}{c_1} - \frac{\phi_0''(r_0)\, R^2}{2\bar{\alpha}c_1}\right)\left(\frac{1+\bar{\alpha}^2 r_0^2}{r_0^2}\right) + \left(\frac{\tilde{\tilde{M}}^2 W_0^2}{2r_0}\right)^2\right\}\bar{P}^* = 0, \tag{5.29}$$

or

$$\bar{P}^*_{\xi\xi} - \left[\tfrac{1}{4}\xi^2 + \frac{\lambda_0 c_2 + \lambda_3}{2(\lambda_1)^{\frac{1}{2}}}\right]\bar{P}^* = 0, \tag{5.30}$$

where

$$\lambda_3 = \left[\frac{\tilde{\tilde{M}}^2 W_0^2}{2r_0}\right]^2. \tag{5.31}$$

Since (5.30) is again a form of Weber's equation, then

$$c_3 = -\left\{\frac{(\lambda_1)^{\frac{1}{2}}(1+2m) + \lambda_3}{\lambda_0}\right\}, \quad m = 0, 1, 2, \ldots. \tag{5.32}$$

Figure 6(*a*) shows a comparison of asymptotic results (solid lines) with numerical results (broken line), for $n = -5, -10, -15$ with $M = |n|^{\frac{3}{8}}$ (i.e. $\tilde{\tilde{M}} = 1$). Again the comparison becomes markedly better as $|n|$ increases. The corresponding distribution of c_r is again good, and shown in figure 6(*b*).

5.4. $M = O(|n|^{\frac{1}{2}})$

In this case it is quite clear from the previous subsection that when $\tilde{\tilde{M}} = O(|n|^{\frac{1}{8}})$, then the c_2 term (see (5.26)), which grows as $\tilde{\tilde{M}}^2$ will become comparable in magnitude to the term involving c_1 (which is independent of $\tilde{\tilde{M}}$); in addition to this, since c_3 grows as $\tilde{\tilde{M}}^4$ as $\tilde{\tilde{M}}$ increases, then this term will also become comparable to the c_1 term when $M = O(|n|^{\frac{1}{2}})$. In this case, it is straightforward to show that $R = O(1)$ remains the appropriate radial scale, whilst the wave speed expands as follows:

$$c = c_0 + \frac{c_1}{n} + \frac{c_2}{|n|^{\frac{3}{2}}} + \ldots, \tag{5.33}$$

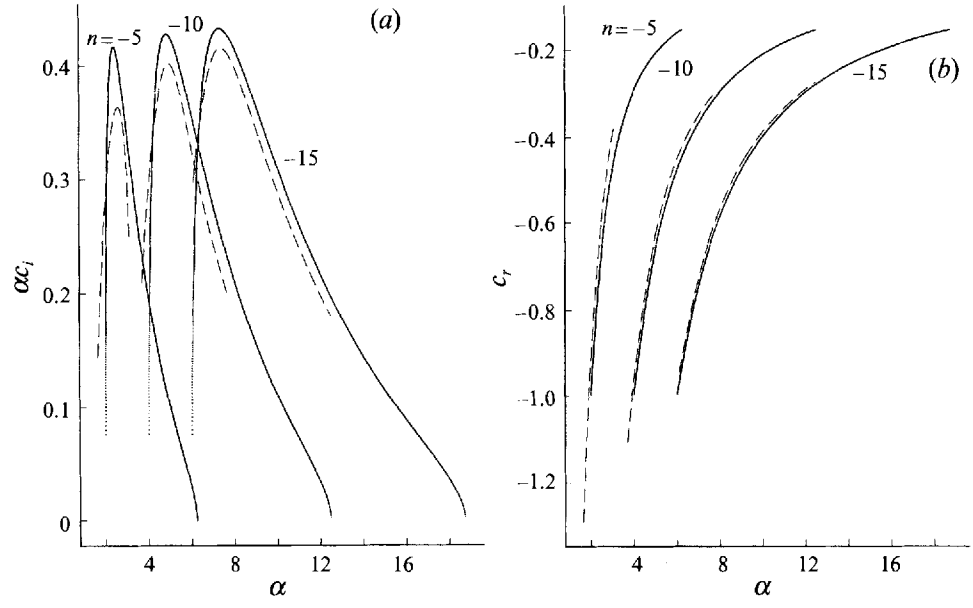

FIGURE 6. Variation of (*a*) growth rate c_i, and (*b*) c_r with α, for $n = -5, -10, -15$, $M = |n|^{\frac{3}{5}}$.

implying
$$\phi = \phi_1 + \frac{\phi_2}{|n|^{\frac{1}{2}}} + \ldots. \tag{5.34}$$

If we write
$$M = |n|^{\frac{1}{4}}\hat{M}, \quad \hat{M} = O(1), \tag{5.35}$$

then the equation for $\bar{P}(R)$ is

$$\bar{P}_{RR} - \hat{P}_R\left[\frac{\hat{M}^2|n|^{\frac{1}{4}}W_0^2}{r_0}\right] - \left\{|n|^{\frac{1}{2}}\left[\left(\frac{(rW)_0' + \bar{\alpha}r_0^2U_0'}{r_0^2\phi_1}\right)\left(\frac{2W_0}{r_0^2\phi_1} - \text{sign}\,(n)\frac{\hat{M}^2W_0^2}{r_0}\right)\right.\right.$$
$$+\left(\frac{1+\bar{\alpha}^2r_0^2}{r_0^2\phi_1}\right)\left(\phi_1 - \frac{(W^2r^2)_0'}{r_0^3\phi_1}\right)\Bigg] + \left[-2\left(\frac{(rW)_0' + \bar{\alpha}r_0^2U_0'}{r_0^2\phi_1}\right)^2\frac{\phi_2}{\phi_1}\right.$$
$$\left.\left. + \text{sign}\,(n)\left(\frac{(rW)_0' + \bar{\alpha}r_0^2U_0'}{r_0^2\phi_1}\right)\left(\frac{\hat{M}^2W_0^2}{r_0}\right)\frac{\phi_2}{\phi_1} + 2\left(\frac{1+\bar{\alpha}^2r_0^2}{r_0^2\phi_1}\right)\left(\frac{(W^2r^2)_0'}{r_0^2\phi_1}\right)\frac{\phi_2}{\phi_1}\right]\right\}\bar{P} = 0. \tag{5.36}$$

Again using a standard transformation of the form
$$\bar{P}(R) = \bar{P}^*(R)\exp\left[\tfrac{1}{2}(|n|^{\frac{1}{4}}\hat{M}^2W_0^2R/r_0)\right], \tag{5.37}$$

leads to the differential equation

$$\bar{P}^*_{RR} - \left\{|n|^2\left[\left(\frac{(rW)_0' + \bar{\alpha}r_0^2U_0'}{r_0^2\phi_1}\right)\left(\frac{2W_0}{r_0^2\phi_1} - \text{sign}\,(n)\frac{\hat{M}^2W_0^2}{r_0}\right)\right.\right.$$
$$+\left(\frac{1+\bar{\alpha}^2r_0^2}{r_0^2\phi_1}\right)\left(\phi_1 - \frac{(W^2r^2)_0'}{r_0^3\phi_1}\right) + \left(\frac{\hat{M}^2W_0^2}{2r_0}\right)^2\Bigg] + \left[-2\left(\frac{(rW)_0' + \bar{\alpha}r_0^2U_0'}{r_0^2\phi_1}\right)^2\frac{\phi_2}{\phi_1}\right.$$
$$\left.\left. + \text{sign}\,(n)\left(\frac{(rW)_0' + \bar{\alpha}r_0^2U_0'}{r_0^2\phi_1}\right)\left(\frac{\hat{M}^2W_0^2}{r_0}\right)\frac{\phi_2}{\phi_1} + 2\left(\frac{1+\bar{\alpha}^2r_0^2}{r_0^2\phi_1}\right)\left(\frac{(W^2r^2)_0'}{r_0^2\phi_1}\right)\frac{\phi_2}{\phi_1}\right]\right\}\bar{P}^* = 0. \tag{5.38}$$

If our assumption regarding the importance of the $R = O(1)$ scale is to be consistent (although see the comments below regarding $R = O(|n|^{\frac{1}{4}})$) then the coefficient involving

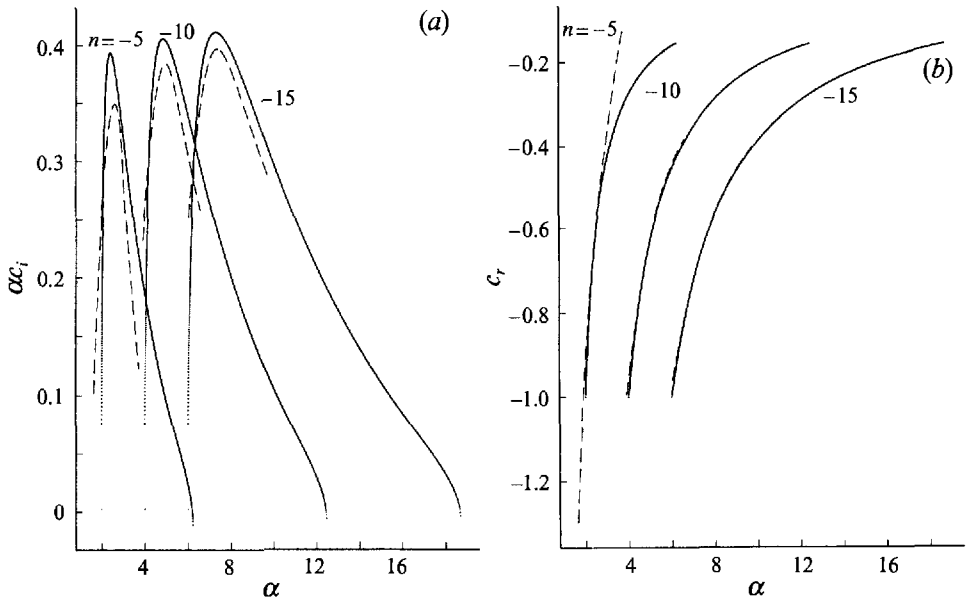

FIGURE 7. Variation of (*a*) growth rate c_i, and (*b*) c_r, with α, for $n = -5, -10, -15$, $M = |n|^{\frac{1}{2}}$.

$|n|^{\frac{1}{2}}$ above must be zero. (This is also consistent with the previous smaller orders of Mach number considered previously.) This leads to

$$c_1 = \frac{-\dfrac{\hat{M}^2 W_0^2}{2\bar{\alpha} r_0}\left(\dfrac{(rW)_0' + \bar{\alpha} r_0^2 U_0'}{1+\bar{\alpha}^2 r_0^2}\right) \pm \left[\left(\dfrac{\hat{M}^2 W_0^2}{2\bar{\alpha} r_0^2}\right)^2 \dfrac{(W^2 r^2)_0' r_0}{1+\bar{\alpha}^2 r_0^2} + c_1^{inc^2}\right]^{\frac{1}{2}}}{1 + \dfrac{1}{1+\bar{\alpha}^2 r_0^2}\left(\dfrac{\hat{M}^2 W_0^2}{2}\right)^2}, \tag{5.39}$$

where c_1^{inc} denotes the incompressible value of c_1, given by (5.12). The equation that determines $\bar{P}(R)$ is then

$$\bar{P}_{RR}^* - \left\{2\left(\frac{c_2}{c_1} - \frac{\phi_0''(r_0)\, R^2}{2\bar{\alpha} c_1}\right)\operatorname{sign}(n)\left[\frac{1+\bar{\alpha}^2 r_0^2}{r_0^2} + \left(\frac{\hat{M}^2 W_0^2}{2r_0}\right)^2 + \operatorname{sign}(n)\frac{W_0^2 \hat{M}^2}{2r_0}\left(\frac{(rW)_0' + \bar{\alpha} r_0^2 U_0'}{r_0^2 \bar{\alpha} c_1}\right)\right]\right\}\bar{P}^* = 0, \tag{5.40}$$

or symbolically

$$\bar{P}_{RR}^* - [\hat{\lambda}_1 R^2 + \hat{\lambda}_0 c_2] = \bar{P}^* = 0, \tag{5.41}$$

and using previous arguments, we must have

$$c_2 = -(\hat{\lambda}_1)^{\frac{1}{2}}(1+2m)/\hat{\lambda}_0, \quad m = 0, 1, 2, \ldots. \tag{5.42}$$

Note that although the transformation (5.37) suggests growth as $R \to \infty$, this is more than offset by the decay of the parabolic cylinder functions, albeit on a larger lengthscale $R = O(|n|^{\frac{1}{4}})$. Note too that the transformation (5.37) is consistent with that used previously, namely (5.28).

Figure 7(*a*) shows a comparison between the above asymptotic results (solid line) and the 'exact' numerical results (broken line), for the most unstable growth rates when $n = -5, -10, -15$ ($M = |n|^{\frac{1}{2}}$, i.e. $\hat{M} = 1$ in all cases). Again the agreement is seen to improve as $-n$ increases. Figure 7(*b*) shows a comparison between the corresponding c_r, for the above cases and indicates good agreement between our asymptotic and numerical results.

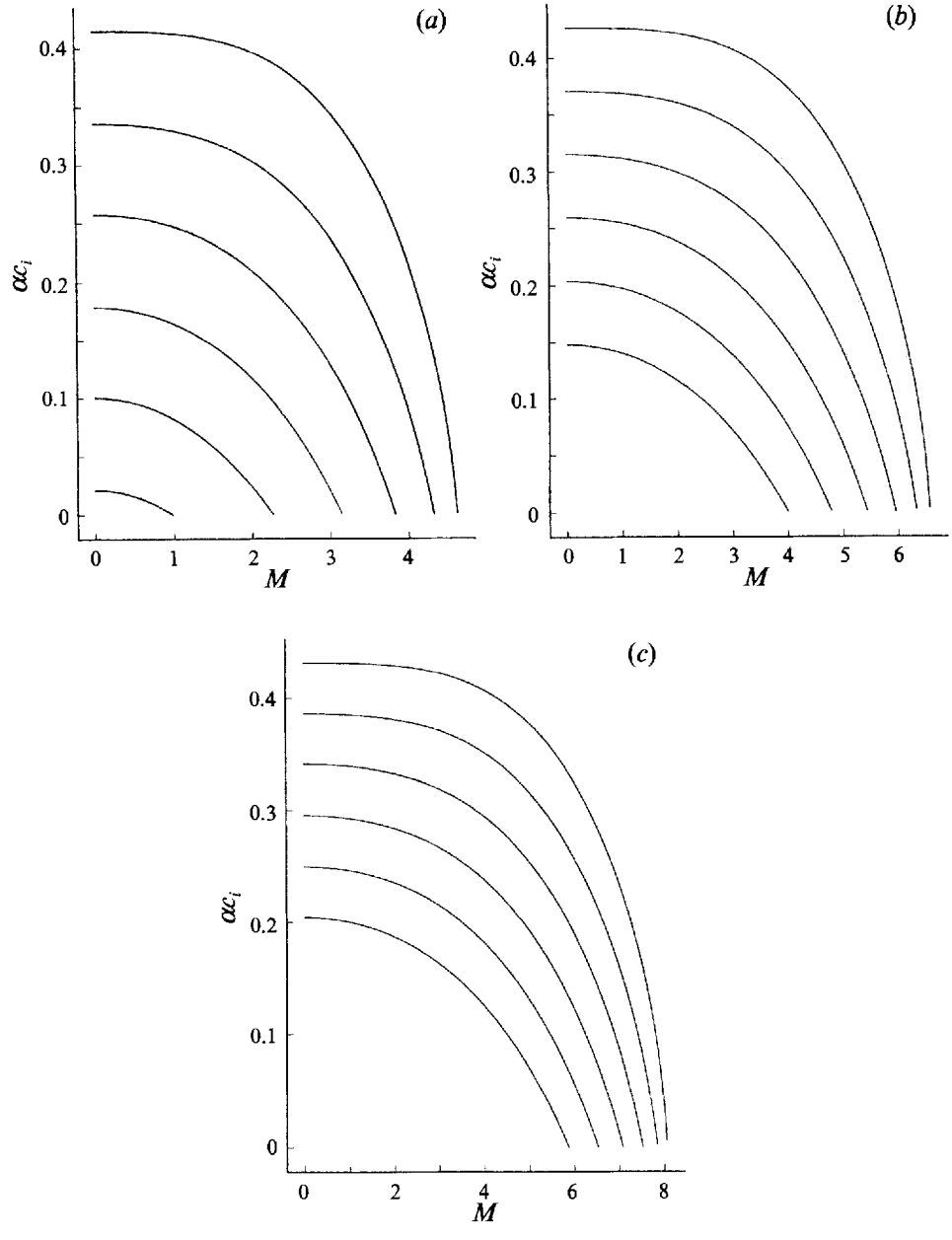

FIGURE 8. Variation of growth rate with M (first 6 modes) using §5.4 results: (*a*) $n = -5$, $\alpha = 2.5$; (*b*) $n = -10$, $\alpha = 5$; (*c*) $n = -15$, $\alpha = 7.5$.

It turns out, however, that this order of M marks a watershed. When $\hat{M}$ is not large, both roots of c_1 must be complex (and from our previous discussions the flow is unstable). As $\hat{M}$ increases, however, eventually terms inside the square-root term in (5.39) will become positive, and hence the two roots of c_1 will cease to be complex-conjugate pairs, but will both become real. In particular, this will occur when

$$\frac{\hat{M}^2 W_0^2}{2\bar{\alpha} r_0^2} \frac{(W^2 r^2)_0' r_0}{1 + \bar{\alpha}^2 r_0^2} = c_1^{inc^2}. \tag{5.43}$$

To illustrate the stabilization of these modes, in figure 8(*a–c*) we show the variation of the growth rates with M for the cases $n=-5$ and $\alpha=2.5$, $n=-10$ and $\alpha=5$, $n=-15$ and $\alpha=7.5$ respectively. We clearly see these modes becoming neutrally stable at finite values of M. For comparison, in figure 9(*a–c*) (corresponding to figure 8*a–c* respectively) we show the corresponding results from solutions of the full system (3.11) and (3.12). At the lower values of M, there is good correlation between the two sets of results. However, as the Mach number increases, and as the order of the modes (i.e. m) increases, the correlation deteriorates. We consider this latter point first by examining the behaviour of the higher-order modes.

5.5. *The structure when* $m = O(|n|^{\frac{1}{2}})$, $(M = O(|n|^{\frac{1}{2}}))$

One detail that has not been considered so far is the behaviour of the modes as m, the index of the Weber function, increases. This feature was considered by Duck (1986), and we consider this aspect here for the important case when $M = O(|n|^{\frac{1}{2}})$. c develops in the same manner as in the previous subsection, and close to the critical layer ϕ takes the form

$$\phi = \phi_1 + \frac{1}{|n|^{\frac{1}{2}}}\phi_2 + \ldots. \tag{5.44}$$

c_0 remains unchanged from that given previously; however c_1 will differ. In this case, we consider the lengthscale

$$\tilde{R} = (r - r_0)|n|^{\frac{1}{2}} = O(1), \tag{5.45}$$

and so on this scale

$$\phi_1 = -\bar{\alpha}c_1 + \tfrac{1}{2}\,\mathrm{sign}\,(n)\,\phi_0''(r_0)\,\tilde{R}^2, \tag{5.46}$$

$$\phi_2 = -\bar{\alpha}c_2 + \frac{\mathrm{sign}\,(n)}{3!}\phi_0'''(r_0)\,\tilde{R}^3. \tag{5.47}$$

Substitution of these expansions into our governing equation gives, to leading order, an eigenfunction equation of the form

$$P_{\tilde{R}\tilde{R}} + q_1(\tilde{R})\,P_{\tilde{R}} + |n| q_2(\tilde{R})\,P = 0. \tag{5.48}$$

Using the standard transformation

$$P(\tilde{R}) = P^*(\tilde{R}) \exp\left[-\frac{1}{2}\int q_1(\tilde{R})\,\mathrm{d}\tilde{R}\right], \tag{5.49}$$

we obtain

$$P^*_{\tilde{R}\tilde{R}} + [|n| q_2 - \tfrac{1}{2}q_{1\tilde{R}} - \tfrac{1}{4}q_1^2]\,P^* = 0. \tag{5.50}$$

However, since $|n|$ is large, (5.50) may be approximated by

$$P^*_{\tilde{R}\tilde{R}} + |n| q_2\,P^* = 0, \tag{5.51}$$

where

$$q_2 = -\frac{1}{r_0^5\phi_1^2}[4r_0 W_0^2 + (1+\bar{\alpha}^2 r_0^2)(r_0^3\phi_1^3 - (W^2 r^2)_0') - \mathrm{sign}\,(n)\,2W_0^2 r_0^2 \hat{M}^2\phi_1 + \tfrac{1}{4}\hat{M}^4 W_0^4 \phi_1^2 r_0^3]. \tag{5.52}$$

Thus (5.50) may be written as

$$P^*_{\xi\xi} + h^2\left[\frac{\mu}{(1+\xi^2)^2} - \frac{\eta}{(1+\xi^2)} - n\right]P^* = 0, \tag{5.53}$$

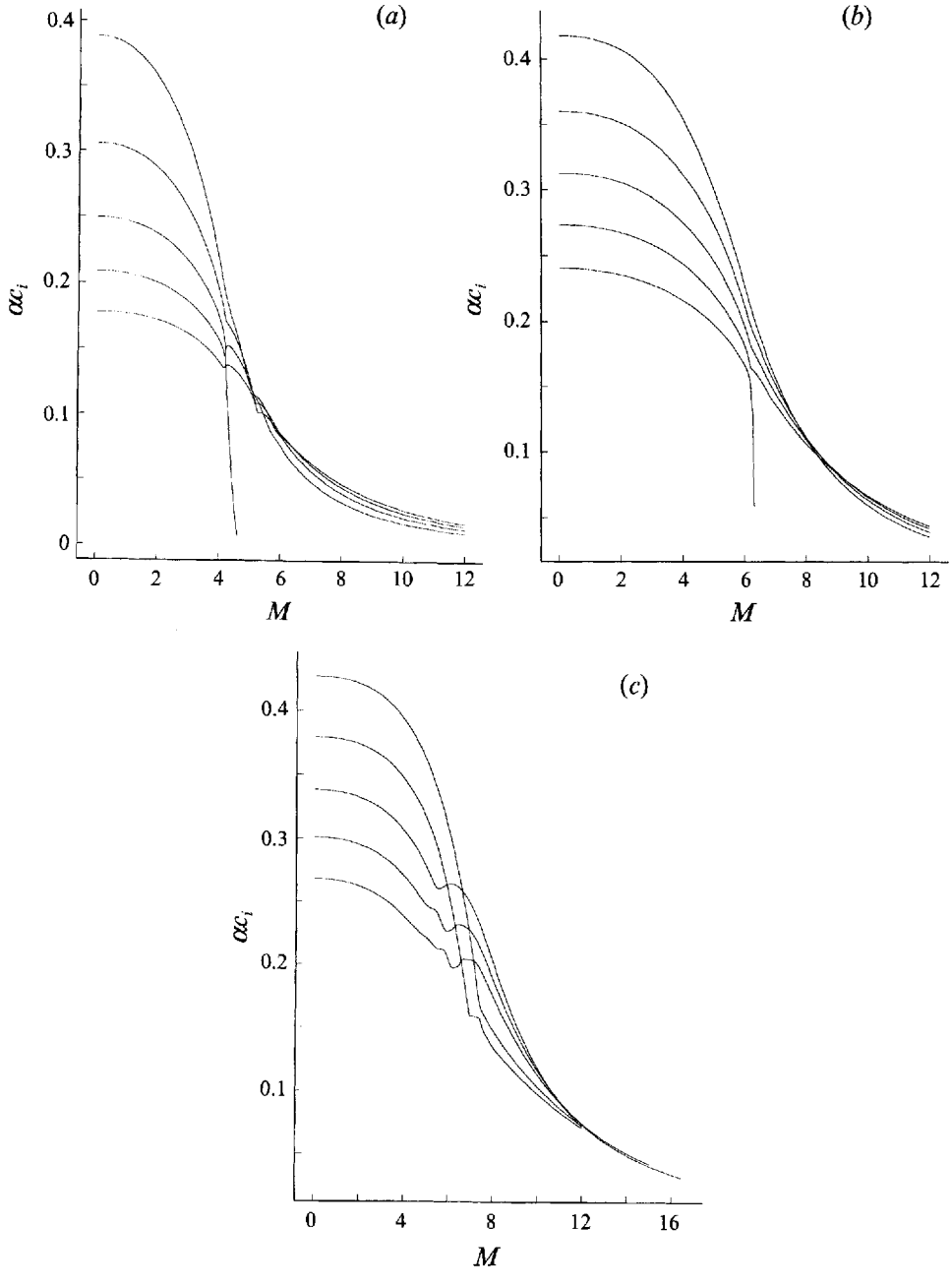

FIGURE 9. Variation of growth rate with M (first 6 modes) fully numerical results: (*a*) $n = -5$, $\alpha = 2.5$; (*b*) $n = -10$, $\alpha = 5$; (*c*) $n = -15$, $\alpha = 7.5$.

with
$$\mu = \frac{2[4r_0 W_0^2 - (1+\bar{\alpha}^2 r_0^2)(W^2 r^2)_0'] \operatorname{sign}(n)}{\bar{\alpha} c_1 r_0^2 \phi_0''(r_0)}, \tag{5.54}$$

$$\nu = \frac{-2[(1+\bar{\alpha}^2 r_0^2) + \hat{M}^4 W_0^4/4]\,\bar{\alpha} c_1 \operatorname{sign}(n)}{r_0^2 \phi_0''(r_0)}, \tag{5.55}$$

$$\eta = \frac{4 W_0^3 \hat{M}^2}{r_0^3 \phi_0''(r_0)}, \tag{5.56}$$

$$\tilde{\xi} = \left[\frac{-\phi_0''(r_0)\operatorname{sign}(n)}{2\bar{\alpha} c_1}\right]^{\frac{1}{2}} \tilde{R}, \tag{5.57}$$

$$h^2 = |n|. \tag{5.58}$$

Equation (5.53) is now in a form suitable for a WKBJ type of approximation. This equation has four turning points; however for the range of $\tilde{\xi}$ required we need consider only the turning points at

$$\tilde{\xi} = \pm\left[-\frac{1}{2}\frac{\eta}{\nu} + \frac{1}{2}\left(\frac{\eta^2}{\nu^2} + \frac{4\mu}{\nu}\right)^{\frac{1}{2}} - 1\right]^{\frac{1}{2}}. \tag{5.59}$$

For large h the WKBJ solution is given by

$$P^* = \tilde{q}^{-\frac{1}{4}}\left[A_1 \exp\int (ih\tilde{q}^{\frac{1}{2}}\,\mathrm{d}\tilde{\xi}) + A_2 \exp\int -(ih\tilde{q}^{\frac{1}{2}}\,\mathrm{d}\tilde{\xi})\right], \tag{5.60}$$

where
$$\tilde{q} = \frac{\mu}{(1+\tilde{\xi}^2)^2} = \frac{\eta}{(1+\tilde{\xi}^2)} - \nu. \tag{5.61}$$

The treatment near the turning points is standard (see for example Duck 1986) and leads to the following dispersion relationship for c_1:

$$Ih = -\tfrac{1}{4}\pi(1+2m), \quad m = 0, 1, 2, \ldots, \tag{5.62}$$

where

$$I = \int_{\tilde{\xi}_1}^{0} \left\{\frac{\mu}{(1+\tilde{\xi}^2)^2} - \frac{\eta}{(1+\tilde{\xi}^2)} - \nu\right\}^{\frac{1}{2}} \mathrm{d}\tilde{\xi}$$

$$= \nu^{\frac{1}{2}} g\left\{-(\tfrac{1}{2}g - \eta/2\nu) F(\tfrac{1}{2}\pi, k) + g_1 E(\tfrac{1}{2}\pi, k) - \frac{\mu}{\nu}\left(\frac{1}{-\frac{1}{2}(\eta/\nu) + \frac{1}{2}g_1}\right) \Pi(\tfrac{1}{2}\pi, \hat{\alpha}^2, k)\right\}, \tag{5.63}$$

$$\tilde{\xi}_1 = \left[-\frac{1}{2}\frac{\eta}{\nu} + \frac{1}{2}\left(\frac{\eta^2}{\nu^2} + \frac{4\mu}{\nu}\right)^{\frac{1}{2}} - 1\right]^{\frac{1}{2}}, \tag{5.64}$$

$$g = \frac{1}{\mathrm{i}[(\eta^2/\nu^2) + (4\mu/\nu)]^{\frac{1}{4}}}, \tag{5.65}$$

$$g_1 = 1/g^2, \tag{5.66}$$

$$k = g(-(\eta/2\nu) + \tfrac{1}{2}g_1 - 1)^{\frac{1}{2}}, \tag{5.67}$$

$$\hat{\alpha}^2 = \frac{-2k^2}{[(\eta/\nu) - g_1]g^2}. \tag{5.68}$$

Here, $F(\frac{1}{2}\pi, k)$, $E(\frac{1}{2}\pi, k)$, $\Pi(\frac{1}{2}\pi, \hat{\alpha}^2, k)$ denote complete elliptic integrals of the first, second and third kinds respectively.

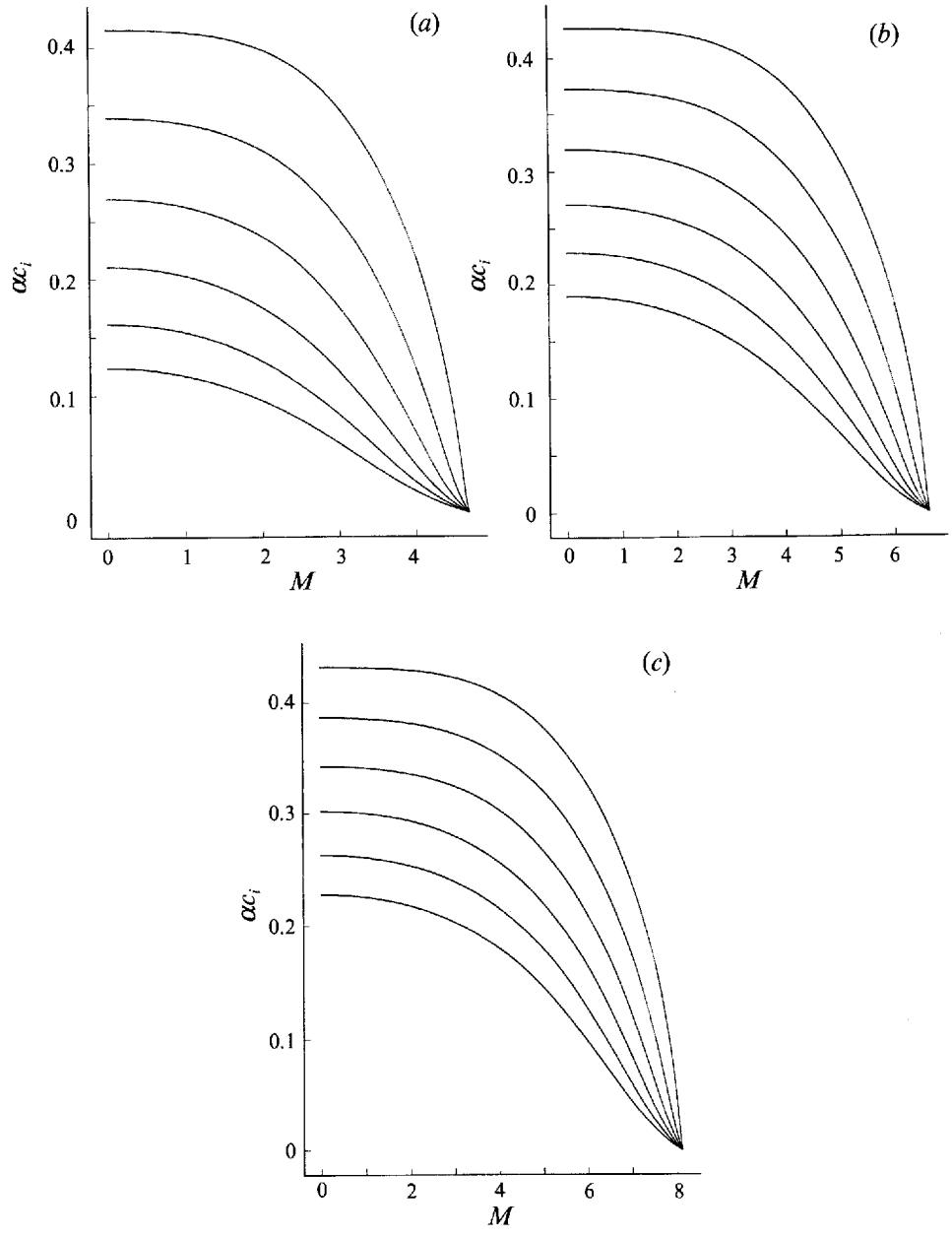

FIGURE 10. Variation of growth rate with M (first 6 modes) using §5.5 results: (*a*) $n = -5$, $\alpha = 2.5$; (*b*) $n = -10$, $\alpha = 5$; (*c*) $n = -15$, $\alpha = 7.5$.

The system (5.62) was solved using Newton iteration, and results for variations of growth rate with M were computed for $m = 0, 1, 2, 3, 4, 5$ for the cases $n = -5$, $\alpha = 2.5$ (figure 10*a*), $n-10$, $\alpha = 5$ (figure 10*b*), $n = -15$, $\alpha = 7.5$ (figure 10*c*). The modified theory of this subsection does indicate some important improvement in the comparison with figure 9; in particular the 'bunching up' of the modes with an increase in order is captured. However, although for $n = -15$ there is quite good correlation for the lower-order modes, as m increases the various wiggles observed in figure 9 are not described, and more importantly our asymptotic results do not capture the instability

shown in figure 9 beyond about $M = 8$. Indeed, figure 9 indicates instability as $\hat{M}$ increases. We therefore conclude that the nature of these modes as $\hat{M} \to \infty$ is somewhat different. It turns out from the analysis of the following section that as $\hat{M} \to \infty$ a further class of mode emerges, somewhat distinct from those considered so far.

6. Centre modes, $M = O(|n|)$

Here we examine modes exhibited when the Mach number is of order n, i.e.

$$M = |n|\bar{M}, \quad \bar{M} = O(1). \tag{6.1}$$

As noted previously, as $M \to \infty$ the features of the modes exhibited at lower Mach numbers cease to exist. In fact the analysis of §5.5 suggests that the modes in this regime under present consideration are neutral. However, our numerics belie this and point towards the existence of *centre modes*, by which we mean that the eigenvalues are determined primarily by conditions close to the axis of the vortex, $r = 0$, in a manner similar to that of Stewartson & Brown (1984, 1985). Here, the complex wave speed develops as

$$c = c_0 + \frac{c_1}{n^2} + \ldots \tag{6.2}$$

(an expansion that can be verified *a posteriori*) and therefore

$$\begin{aligned} \phi &= n\phi_0 + \frac{\phi_1}{n} + \ldots \\ &= n\left\{\bar{\alpha}(U - c_0) + \frac{W}{r}\right\} + \frac{1}{n}\{-\bar{\alpha}c_1 + \tfrac{1}{2}\phi_0''(0)\, r^2\} + \ldots . \end{aligned} \tag{6.3}$$

In order to be consistent we must have that $\phi_0(r = 0) = 0$, i.e.

$$c_0 = 1 + q/\bar{\alpha}. \tag{6.4}$$

We must now go on to find c_1 in our complex wave-speed expansion. The flow is divided into the four regions, which are considered in turn.

We first begin our analysis at the outer region of the flow, where $r = O(1)$, and the governing equation has the form

$$P_{rr} - n^2 \frac{W^2\bar{M}^2}{r} P_r + n^4 \bar{M}^2 \phi_0^2 P = 0. \tag{6.5}$$

Using a transformation of the form

$$P = P^*(r) \exp\left\{\int_{\tilde{r}_0}^{r} \frac{n^2 W^2 \bar{M}^2}{2r}\, \mathrm{d}r\right\}, \tag{6.6}$$

and writing

$$\chi_0 = -\bar{M}^2\phi_0^2 + W^4\bar{M}^4/4r^2, \tag{6.7}$$

reduces (6.5) to

$$P^*_{rr} - n^4 \chi_0 P^* = 0. \tag{6.8}$$

We define the critical point $\tilde{r}_0$ by $\chi_0(\tilde{r}_0) = 0$ and when $r > \tilde{r}_0$, $\chi_0 < 0$ and the approximate solution to (6.8) is given by

$$P^* = \frac{E_1}{[-\chi_0]^{\frac{1}{4}}} \exp\left\{\mathrm{i}n^2 \int_{\tilde{r}_0}^{r} [-\chi_0]^{\frac{1}{2}}\, \mathrm{d}r\right\}, \tag{6.9}$$

where E_1 is an unknown constant.

We have also assumed that $[-\chi_0]^{\frac{1}{3}}$ is slightly imaginary, with its imaginary part positive. This condition is to ensure that the solution is bounded as $r \to \infty$, otherwise if $\mathrm{Im}\{[-\chi_0]^{\frac{1}{3}}\} < 0$ we replace i by $-$i in (6.9). Looking at this point from a more physical perspective, we require waves to propagate out from the critical layer and not in toward it.

In order to be able to match (6.9) with the solution in the $r < \tilde{r}_0$ region, we must first examine the solution of the flow in the transition layer, around $r = \tilde{r}_0$. The lengthscale in this region turns out to be

$$r - \tilde{r}_0 = \hat{R}|n|^{-\frac{4}{3}}, \quad \hat{R} = O(1), \tag{6.10}$$

and use of this scaling reduces our governing equation to the Airy equation, which has solutions of the form

$$P^* = F_1 \,\mathrm{Ai}((\chi_0'(\tilde{r}_0))^{\frac{1}{3}}\hat{R}) + F_2 \,\mathrm{Bi}((\chi_0'(\tilde{r}_0))^{\frac{1}{3}}\hat{R}). \tag{6.11}$$

Standard analysis and matching with (6.9) yields the result

$$F_1 = \mathrm{i}F_2. \tag{6.12}$$

In the region $r < \tilde{r}_0, \chi_0 > 0$ and hence the WKBJ solution here is given by

$$P^* = \frac{1}{\chi_0^{\frac{1}{4}}}\left\{D_1 \exp\left\{\int_{\tilde{r}_0}^{r} n^2\left[\frac{W^4\bar{M}^4}{4r^2} - \bar{M}^2\phi_0^2\right]^{\frac{1}{2}} \mathrm{d}r\right\}\right.$$
$$\left. + D_2 \exp\left\{-\int_{\tilde{r}_0}^{r} n^2\left[\frac{W^4\bar{M}^4}{4r^2} - \bar{M}^2\phi_0^2\right]^{\frac{1}{2}} \mathrm{d}r\right\}\right\}. \tag{6.13}$$

As we approach the transition layer this solution must match with (6.11) implying

$$D_1 = -2\mathrm{i}D_2. \tag{6.14}$$

Here we have used the property that Bi(z) has no exponentially small component along the positive real axis (Berry 1989). Note that as $r \to 0$

$$P^* \sim \frac{\sqrt{2}}{q\bar{M}r^{\frac{1}{2}}}\{D_1 Z_1 \exp(\tfrac{1}{4}q^2\bar{M}^2r^2n^2) + D_2 Z_2 \exp(-\tfrac{1}{4}q^2\bar{M}^2r^2n^2)\}, \tag{6.15}$$

where

$$Z_1 = \exp\left\{\int_{\tilde{r}_0}^{0} n^2(\chi_0^{\frac{1}{2}})\,\mathrm{d}r\right\}, \tag{6.16}$$

$$Z_2 = 1/Z_1. \tag{6.17}$$

We now consider the lengthscale, $r = O(|n|^{-\frac{1}{2}})$, by setting

$$\bar{r} = r|n|^{\frac{1}{2}} = O(1). \tag{6.18}$$

The governing equation in this region, to leading order, is given by

$$P_{\bar{r}\bar{r}} - |n|q^2\bar{M}^2\bar{r}P_{\bar{r}} + n^2\left[\frac{2q^3\bar{M}^2}{\phi_1} - \frac{1}{\bar{r}^2}\right]P = 0, \tag{6.19}$$

where

$$\phi_1 = \tfrac{1}{2}\phi_0''(0)\,\bar{r}^2, \tag{6.20}$$

and as previously it is necessary to use a transformation, which is of the standard type, i.e.

$$P = P^{**}\exp\left\{\frac{1}{2}\int |n|q^2\bar{r}\bar{M}\,\mathrm{d}\bar{r}\right\}, \tag{6.21}$$

which leads to the final form of the governing equation in this region, namely

$$P^{**}_{\bar{r}\bar{r}} + n^2\left[\frac{2q^3\bar{M}^2}{\frac{1}{2}\phi_0''(0)\,\bar{r}^2} - \frac{1}{\bar{r}^2} - \tfrac{1}{4}q^4\bar{r}^2\bar{M}^4\right]P^{**} = 0. \tag{6.22}$$

This equation yields solutions of the form

$$P^{**} = \bar{r}^{\frac{1}{2}}(C_1 I_\nu(\tfrac{1}{4}q^2\bar{M}^2|n|\bar{r}^2) + C_2 K_\nu(\tfrac{1}{4}q^2\bar{M}^2|n|\bar{r}^2)), \tag{6.23}$$

where I_ν and K_ν are modified Bessel functions, written in standard form, with

$$\nu = \tfrac{1}{2}|n|\left(1 - \frac{2q^3\bar{M}^2}{\frac{1}{2}\phi_0''(0)}\right)^{\frac{1}{2}}. \tag{6.24}$$

Now, as $\bar{r} \to \infty$

$$P^{**} \sim \frac{C_1\bar{r}^{\frac{1}{2}}}{(2\pi(\frac{1}{4}q^2\bar{M}^2|n|\bar{r}^2))^{\frac{1}{2}}}\exp(\tfrac{1}{4}q^2\bar{M}^2|n|\bar{r}^2) + C_2\bar{r}^{\frac{1}{2}}\left(\frac{\pi}{2(\frac{1}{4}q^2\bar{M}^2|n|\bar{r}^2)}\right)^{\frac{1}{2}}\exp(-\tfrac{1}{4}q^2\bar{M}^2|n|\bar{r}^2) \tag{6.25}$$

(these results arise from the large-order large-argument behaviour of Bessel functions, Abramowitz & Stegun 1970, p. 378) and comparing this with (6.15), we see that in order for these solutions to match and taking into account (6.14), then

$$C_1 = -2\mathrm{i}\pi Z_1^2 C_2. \tag{6.26}$$

Here we have that $|C_2| \gg |C_1|$, and thus it is admissible to neglect any exponentially decaying component of the $I_\nu(z)$ Bessel function as $z \to \infty$, which must be exponentially smaller than the corresponding component arising from $K_\nu(z)$; an analogous procedure was adopted by Smith & Brown (1990). Also, we take note of the fact that as $\bar{r} \to 0$ (using the large-order small limit of the large argument property of Bessel functions, Abramowitz & Stegun 1970, p. 378), then

$$P^{**} \sim \bar{r}^{\frac{1}{2}}\tfrac{1}{2}C_2(\tfrac{1}{2}b_1\bar{r}^2)^{-\nu}\mathrm{e}^{-\nu}\nu^{\nu-\frac{1}{2}}(2\pi)^{\frac{1}{2}}, \tag{6.27}$$

where $\beta_1 = \frac{1}{4}q^2\bar{M}^2|n|$ and Sterling's formula has been used to approximate the Gamma function. Next we set

$$R = r|n| = O(1), \tag{6.28}$$

and in this regime ϕ develops as

$$\begin{aligned}\phi &= \frac{\phi_1}{n} + \ldots \\ &= \frac{1}{n}(-\bar{\alpha}c_1 + \tfrac{1}{2}\phi_0''(0)\,R^2) + \ldots,\end{aligned} \tag{6.29}$$

with the governing equation

$$P_{RR} + n^2\left[\frac{4\bar{\alpha}^2q^2 + 4\bar{\alpha}q}{[-\bar{\alpha}c_1 + \frac{1}{2}\phi_0''(0)\,R^2]^2} + \frac{2q^3\bar{M}^2}{[-\bar{\alpha}c_1 + \frac{1}{2}\phi_0''(0)\,R^2]} - \frac{1}{R^2}\right]P = 0, \tag{6.30}$$

which has the solution

$$P = \frac{(\Upsilon R^2)^{\frac{1}{2}|n|+\frac{1}{4}}}{(1-\Upsilon R^2)^{\hat{\mu}}}F(\varpi_1; \varpi_2; |n|+1; \Upsilon R^2), \tag{6.31}$$

where F is the hypergeometric function in standard notation, and

$$\Upsilon = \tfrac{1}{2}\phi_0''(0)/\bar{\alpha}c_1, \quad \varpi_1 = \tfrac{1}{2}(|n|-s) - \hat{\mu}, \quad \varpi_2 = \tfrac{1}{2}(|n|+s) - \hat{\mu}, \tag{6.32a–c}$$

$$s = (n^2+b)^{\frac{1}{2}}, \quad \hat{\mu}(\hat{\mu}+1) = -\tfrac{1}{4}a\Upsilon, \tag{6.32d, e}$$

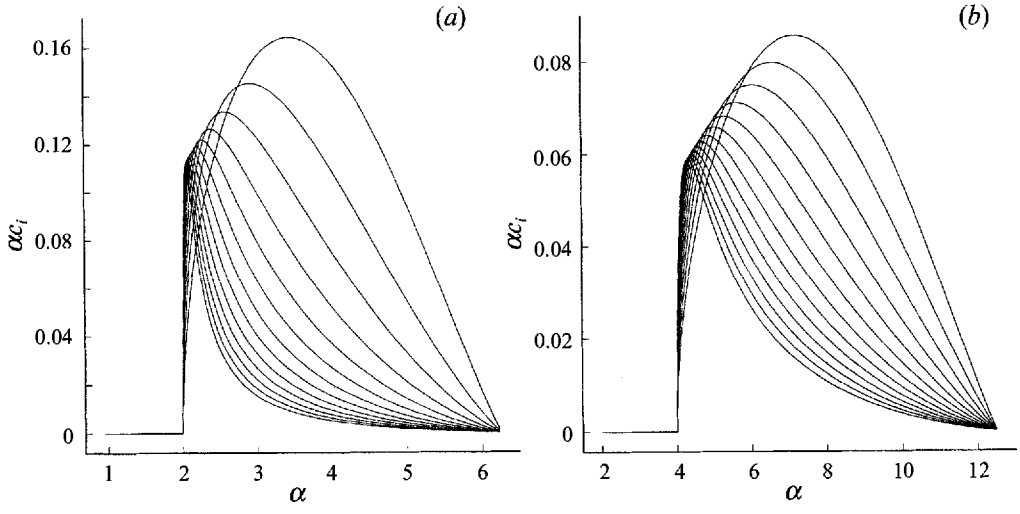

FIGURE 11. Variation of growth rate with α for centre modes: (*a*) $n = -5$, $M = 5$; (*b*) $n = -10$, $M = 10$.

with
$$a = n^2\left\{\frac{4q\bar{\alpha}+4q^2\bar{\alpha}^2}{\frac{1}{4}(\phi_0''(0))^2}\right\}, \quad b = \frac{4q^3|n|^2\bar{M}^2}{\phi_0''(0)}. \tag{6.33a, b}$$

Note that this equation is very similar in form to that found by Stewartson & Capell (1985). This solution is valid for $R = O(1)$ and all smaller orders, and, in particular is finite at $R = 0$ by the definition of the hypergeometric function, and therefore satisfies our boundary conditions at the centre of the vortex. Note, however, that although according to the above $P = O(R^{|n|+\frac{1}{2}})$ as $R \to 0$ whilst strictly we should have that $P = O(R^{|n|})$, this discrepancy can be remedied by taking higher-order terms in (6.30); since the above is asymptotically correct as $|n| \to \infty$, and the additional terms are of little consequence to our analysis (indeed they merely cause additional complication), we shall consider them no further. As R becomes large we have

$$P \sim \frac{(\Upsilon R^2)^{\frac{1}{2}|n|+\frac{1}{4}}}{(1-\Upsilon R^2)^{\hat{\mu}}}[s_0(-\Upsilon R^2)^{\hat{\mu}-\frac{1}{2}|n|+\frac{1}{2}s}\Sigma_1 + \delta_0(-\Upsilon R^2)^{\hat{\mu}-\frac{1}{2}|n|-\frac{1}{2}s}\Sigma_2], \tag{6.34}$$

where
$$s_0 = \frac{|n|!(s-1)!}{(\frac{1}{2}|n|+\frac{1}{2}s-\hat{\mu}-1)!(\frac{1}{2}|n|+\frac{1}{2}s+\hat{\mu})!}, \tag{6.35a}$$

$$\delta_0 = \frac{|n|!(-s-1)!}{(\frac{1}{2}|n|-\frac{1}{2}s-\hat{\mu}-1)!(\frac{1}{2}|n|-\frac{1}{2}s+\hat{\mu})!}, \tag{6.35b}$$

and Σ_1 and Σ_2 are both power series expansions in $1/\Upsilon R^2$, with their leading-order terms both unity. Matching the two large-R solutions with (6.27) requires that the coefficient of the growing term in (6.34), namely s_0, must be zero to leading order. Hence we see that $\frac{1}{2}(|n|+s)-\tilde{\mu}$ must either be a negative integer or zero, i.e.

$$\tilde{\mu} = \tfrac{1}{2}(|n|+s)+N, \tag{6.36}$$

for $N = 0, 1, 2 \ldots$.

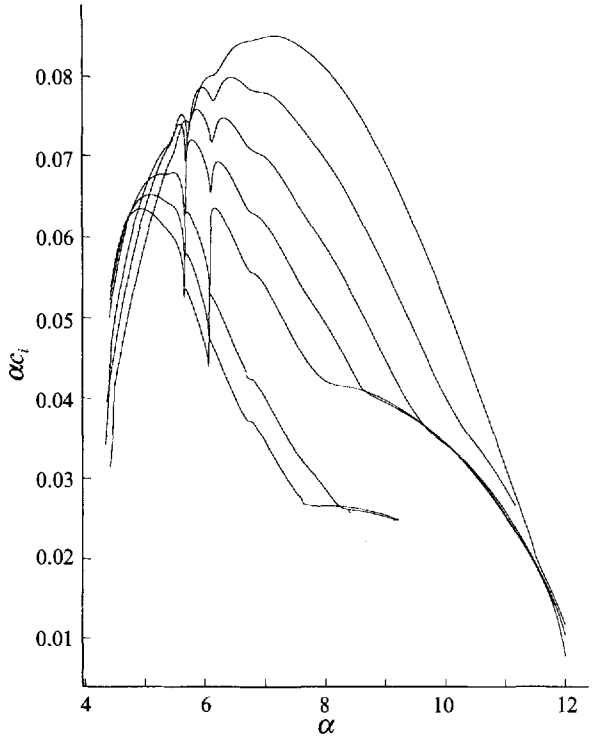

FIGURE 12. Variation of growth rate with α for $n = -10$, $M = 10$, fully numerical results.

Since in our case s (and also ν) is imaginary (unlike the corresponding term in Stewartson & Brown 1985), the above expression substituted into (6.32e and a) yields the leading-order complex contribution to c_1, which is given by

$$c_1 = -\frac{a\phi_0''(0)}{8\bar{\alpha}\hat{\mu}(\hat{\mu}+1)}. \tag{6.37}$$

In figure 11(a) we show the variation of the growth rate with α for the case $n = -5$, $M = 5$. This figure is to be compared with figure 2(e), computed from the full system; comparison between the asymptotic and fully numerical results is surprisingly good, considering the smallness of $-n$ and M. Figure 11(b) shows the growth-rate variation, predicted from the analysis of this subsection, for the case $n = -10, M = 10$ and is to be compared with the fully numerical results shown in figure 12. Again, the results are encouraging; in particular the magnitude and location of the maximum growth rate is quite accurately predicted.

We now present some further numerical evidence for the structure of the centre modes. Figure 13 shows the variation of $\mathrm{Re}\{\phi(r=0)\}$ with M, for the (discrete) points $n = -M$, $\alpha = 0.7M$ (first mode), which points to this quantity tending to zero as M increases. Figure 14 shows the eigensolution for P for the particular case $M = 10$, $n = -10$, $\alpha = 7$, $q = 0.8$ (first mode). On this figure the location of the point where $\mathrm{Re}\{-\bar{M}^2\phi^2 + W^4\bar{M}^4/4r^2\} = 0$ is marked with a circle. The distribution on figure 17 strongly indicates growth in the eigensolution at values of r below this point. Further close inspection of the solution as r increases indicates some relatively small-amplitude oscillations, in accordance with our theory above.

Referring again to figure 11, we see that the upper neutral point is clearly seen. This

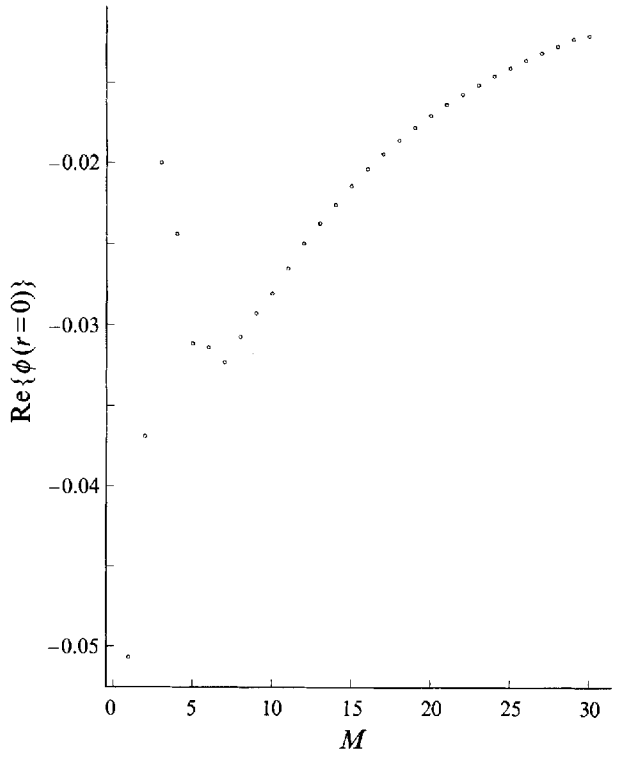

FIGURE 13. Variation of $\mathrm{Re}\{\phi(r=0)\}$ with M, $n=-M$, $\alpha=0.7M$, $q=0.8$, first mode.

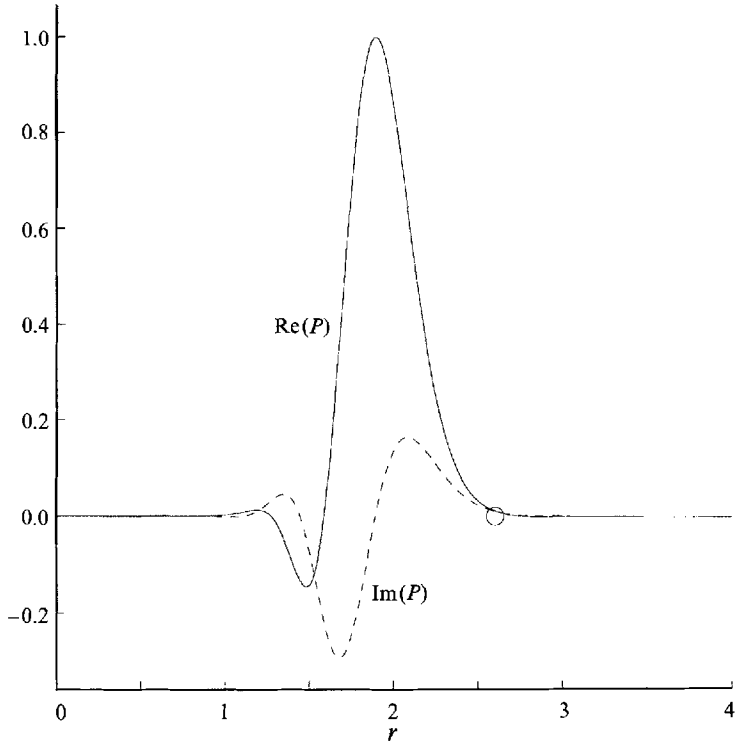

FIGURE 14. P eigensolution for $M=10$, $n=-10$, $\alpha=7$, first mode.

occurs at $\alpha = -n/q$, the point at which $a = 0$ (see (6.33)). The fully numerical results throughout this paper all indicate that neutral conditions are attained at values of the parameters close to this point, as in the incompressible case.

Additionally figure 11 shows a distinct lower neutral point. This corresponds to the value of α where $\phi_0''(0) = 0$ namely $\bar{\alpha} = -\frac{1}{2}q$. At this location, a and b (defined by (6.33)) both exhibit a singularity, although it is easy to show that at this location, $c_1 = (2-q^2)/q^2\bar{M}^2$, which is clearly real. There is some correlation with these results and those of the fully numerical scheme, whilst it is most remarkable that the location of this lower neutral point is identical with that found in the incompressible case (Stewartson & Leibovich 1987), and that both the upper and lower neutral points are captured by (6.37).

It is also worth noting that there is some similarity between the structure of these modes, and those found in the incompressible work of Stewartson & Brown (1985), although the particular details are different, and in our case analytic/asymptotic solution on the $r = O(1)$ scale is possible (see (6.6)), whilst Stewartson & Brown (1985) had to resort to a numerical approach for this scale.

7. Conclusions

We have mounted a systematic study of the inviscid stability of the trailing line vortex, starting at zero Mach number M and progressively increasing M. We see a general reduction in growth rates as M increases, and indeed the results of §§5.4 and 5.5 predict that the original family of modes will stabilize when $M = O(|n|^{\frac{1}{2}})$, specifically when (5.43) is satisfied. However, it is shown in §6 that when $M = O(|n|)$, a centre-mode class of instability is formed. We feel that although our numerical results (figure 9 in particular) indicates that these modes spring from the higher-order modes at lower Mach numbers, as $-n$ increases these centre modes may well become distinct from the original class of modes that exist at lower Mach numbers.

A further important feature of note, and one that is observed in incompressible work (Leibovich & Stewartson 1983; Stewartson & Brown 1985) is that there is a good deal of numerical evidence to suggest that there exist no instabilities for $\alpha > -n/q$. Indeed, this is also confirmed by (6.37), noting that a is given by (6.33). This aspect is currently under further investigation, as are the effects of viscosity when incorporated into the theory. Additionally it is anticipated that non-parallel effects would be of much interest when incorporated into the study.

This research was supported by the National Aeronautics and Space Administration under NASA Contract No. NASA-18605 while one of the authors was in residence at the Institute for Computer Applications in Science and Engineering (ICASE), NASA Langley research centre, Hampton, VA. J.A.K.S. was in receipt of an SERC studentship. A number of the computations were performed with the computer facilities provided by the University of Manchester and SERC. The helpful comments of the referees are also gratefully acknowledged.

REFERENCES

ABRAMOWITZ, M. & STEGUN, I. A. 1970 *Handbook of Mathematical Functions*. Dover.

BATCHELOR, G. K. 1964 Axial flow in trailing line vortices. *J. Fluid Mech.* **20**, 645.

BERRY, M. V. 1989 Uniform asymptotic smoothing of Stokes's discontinuities. *Proc. R. Soc. Lond.* A **422**, 7.

COLEMAN, C. S. 1989 The stability of swirling jets. *Astro. Soc. Austral. Proc.* **8**, 38.

DUCK, P. W. 1986 The inviscid stability of a swirling flow: large wavenumber disturbance. *Z. Angew. Math. Phys.* **37**, 340.

DUCK, P. W. & FOSTER, M. R. 1980 The inviscid stability of a trailing line vortex. *Z. Angew. Math. Phys.* **31**, 524.

DUCK, P. W. & KHORRAMI, M. R. 1991 A note on the effects of viscosity on the stability of a trailing line vortex. *ICASE Rep.* 91-6. (Also *J. Fluid Mech.* **245**, 175, 1992.)

FOSTER, M. R. & DUCK, P. W. 1982 Inviscid stability of Long's vortex. *Phys. Fluids* **25**, 1715.

FOSTER, M. R. & SMITH, F. T. 1989 Stability of Long's vortex at large flow force. *J. Fluid Mech.* **206**, 405.

GÖRTLER, H. 1954 Theoretical investigations of laminar boundary-layer problems II – theory of swirl in an axially symmetric jet, far from the orifice. *Air Force Contract AF* 61(514) 627C.

KHORRAMI, M. R. 1991 On the viscous modes of instability of a trailing line vortex. *J. Fluid Mech.* **225**, 197.

KHORRAMI, M. R., MALIK, M. R. & ASH, R. I. 1989 Application of spectral collocation techniques to the stability of swirling flows. *J. Comput. Phys.* **81**, 206.

LEIBOVICH, S. & STEWARTSON, K. 1983 A sufficient condition for the instability of columnar vortices. *J. Fluid Mech.* **126**, 335.

LESSEN, M. & PAILLET, F. 1974 The stability of a trailing line vortex. Part 2. Viscous theory. *J. Fluid Mech.* **65**, 769.

LESSEN, M., SINGH, P. & PAILLET, F. 1974 The stability of a trailing line vortex. Part 1. Inviscid theory. *J. Fluid Mech.* **63**, 753.

LOITSYANSKII, L. G. 1953 Propagation of a rotating jet in an infinite space surrounded by the same liquid. *Prik. Mat. Mehk.* **17**, 3.

LONG, R. R. 1961 A vortex in an infinite fluid. *J. Fluid Mech.* **11**, 611.

MAYER, E. W. & POWELL, K. G. 1992 Viscous and inviscid instabilities of a trailing vortex. *J. Fluid Mech.* **245**, 91.

MICHALKE, A. 1971 Instabilität eines kompressiblen runden Freistrahls unter Berucksichtigung des Einflusses den Strahlgrenzschtdicke. *J. Flugwiss* **19**, 319.

MICHALKE, A. 1984 Survey on jet instability theory. *Prog. Aerospace Sci.* **21**, 519.

SMITH, F. T. & BROWN, S. N. 1990 The inviscid instability of a Blasius boundary layer at large values of the Mach number. *J. Fluid Mech.* **219**, 499.

STEWARTSON, K. & BROWN, S. N. 1984 Inviscid centre-modes and wall-modes in the stability theory of swirling Poiseuille flow. *IMA J. Appl. Maths* **32**, 311.

STEWARTSON, K. & BROWN, S. N. 1985 Near neutral centre modes as inviscid perturbations to a trailing line vortex. *J. Fluid Mech.* **156**, 387.

STEWARTSON, K. & CAPELL, S. 1985 On the stability of ring modes in a trailing line vortex: the upper neutral points. *J. Fluid Mech.* **156**, 369.

STEWARTSON, K. & LEIBOVICH, S. 1987 On the stability of a columnar vortex to disturbances with large azimuthal wavenumber: the lower neutral points. *J. Fluid Mech.* **178**, 549.